Tikrit Journal of Engineering Sciences (2025); 32(3): 1244
DOI: http://doi.org/10.25130/tjes.32.3.35

IRAQI Academic Scientific Journals

ISSN: 1813-162X (Print); 2312-7589 (Online)

Tikrit Journal of Engineering Sciences

available online at: http://www.tj-es.com

TJES Tikrit Journal of Engineering Sciences

The Influence of Construction Joints on the Shear Behavior of Reinforced Self-Compacting Concrete Beams

Muhaj M. Abdulmunaam *[a], **Omar Shamal Farhan** [b]

[a] Ministry of Construction, Housing and Public Municipalities, Baghdad, Iraq.
[b] Department of Architecture, Al-Nahrain University, Baghdad, Iraq.

Keywords:

Construction joint; Dowels (Shear Connectors); Finite element analysis; Secondary reinforcement; Self-compacting concrete.

Highlights:

- *Horizontal construction joints used with reinforced self-compacted concrete beams.*
- *A Parametric study employing high-strength concrete was done using the ANSYS program.*
- *Stiffness of reinforced beams with the existence of construction joins at different levels.*
- *Higher compressive strength gives less ductile behavior, i.e., great rigidity characteristics in the presence of construction joints.*

ARTICLE INFO

Article history:

Received	24 June 2023
Received in revised form	25 Sep. 2023
Accepted	07 Sep. 2024
Final Proofreading	28 Nov. 2024
Available online	28 Aug. 2025

Citation: Abdulmunaam MM, Farhan OS. **The Influence of Construction Joints on the Shear Behavior of Reinforced Self-Compacting Concrete Beams**. *Tikrit Journal of Engineering Sciences* 2025; **32**(3): 1244.
http://doi.org/10.25130/tjes.32.3.35

*Corresponding author:

Muhaj M. Abdulmunaam

Ministry of Construction, Housing and Public Municipalities, Baghdad, Iraq.

Abstract: Construction joints are essential in massive concrete structures since these structures cannot be cast in a single pour. Nowadays, Self-compacting concrete is preferred due to its ability to compact without vibration and segregation concerns. The present research investigates the shear behavior of reinforced self-compacting concrete beams at the horizontal construction joint regions experimentally and analytically. The experimental works included testing twelve beams to investigate the effect of five test variables: construction joint position, compressive strength, main reinforcement, secondary reinforcement ratios, and the presence of dowels (shear connectors). Strain gauges were used in three locations to investigate the stress in the reinforcing bars. Tests showed that self-compacting concrete beams behave similarly to conventional concrete beams and self-compacting concrete beams without construction. That, the bottom of the compression zone was the optimum level for the construction joints. Increasing compressive strength reduced deflection. In addition, increasing the main reinforcement changed the failure mode from flexural to shear, separating the construction joint. While changing the secondary reinforcement results in totally different behavior since increasing secondary reinforcement changed the failure mode to flexural failure. While decreasing secondary reinforcement resulted in separation at the construction joint level. The results also showed that employing dense dowels impacted ductility because the deflection was reduced. While utilizing fewer dowels insignificantly affected the beam behavior. Further analytical investigations using finite element analysis (ANSYS program) were conducted to study the influence of utilizing high-strength concrete and the secondary reinforcement ratio on the behavior of reinforced self-compacting concrete beams. The analytical results indicated that the shear strength of self-compacting concrete beams was increased with the concrete strength and the secondary reinforcement ratio. Utilizing a 70 MPa high-strength concrete resulted in a 47.4 % ultimate load over the experimental value for regular-strength concrete (28 MPa). Increasing the ratio of secondary reinforcement (0.01229 to 0.049) resulted in a 10.3% increase in ultimate load magnitude. While decreasing the ratio of secondary reinforcement (0.01229 to 0.0025) with spanning the spacing between stirrups reduced the ultimate load magnitude by 55.8%.

تأثير المفاصل الانشائية على سلوك القص للعتبات الخرسانية ذاتية الرص مسلحة

مهج مصطفى عبدالمنعم[1]، عمر شمال فرحان[2]

[1] وزارة الاعمار والاسكان والبلديات العامة / بغداد – العراق.

[2] قسم هندسة العمارة/ جامعة النهرين / بغداد – العراق.

الخلاصة

فواصل البناء الانشائية: هي فواصل بين صب الخرسانة المتسلسلة، وهي ضرورية في الإنشاءات الخرسانية الكتلوية حيث لا يمكن صب هذه الهياكل مرة واحدة. الخرسانة ذاتية الرص: وهي خرسانة مطورة حديثًا ومناسبة تمامًا لمجموعة متنوعة من تطبيقات البناء، لا سيما تلك التي تتطلب مقاومة مبكرة عالية. نظرًا لأن هذا النوع من الخرسانة له قابلية عالية للتدفق وقيمة تشغيلية، فإنه يتيح إنتاج قوالب خرسانية بنسب تسليح عالية دون خوف من الفصل (الانعزال)، حيث لا يحتاج إلى أي اهتزاز لأنه يتماسك تحت تأثير وزنه فقط. الهدف من هذا البحث هو دراسة التأثير التجريبي والنظري للمفاصل الانشائية الأفقية على سلوك القص للعتبات الخرسانية المسلحة ذاتية الرص. تضمنت الأعمال التجريبية صب وفحص اثنا عشرة عتبة لدراسة تأثير خمسة متغيرات اختبارية وهي: موضع المفصل الانشائي وقوة الانضغاط للخرسانة ونسبة حديد التسليح الرئيسي و نسبة حديد التسليح الثانوي ووجود الاوتاد (مسامير القص) التي تربط بين الطبقات الخرسانية عند المفصل الانشائي. تم استخدام مقاييس الانفعال في ثلاثة مواضع مختلفة لقياس الاجهاد في قضبان التسليح القص والانحناء. أظهرت الاختبارات العملية أن سلوك العتبات الخرسانية المسلحة ذاتية الرص يشبه إلى حد كبير سلوك العتبات الخرسانية العادية والعتبات ذاتية الرص المصبوبة بدون حصول فواصل انشائية . تم الاستنتاج بان منطقة الضغط هي المستوى الأمثل للمفصل الانشائي، وان زيادة مقاومة انضغاط الخرسانة ادت الى نقصان في قيمة الهطول. يؤدي تغيير نسبة التسليح الرئيسية الى تحويل نوع الفشل الى (فشل قطري وانفصال في مستوى المفصل الانشائي) في حين تغيير نسب التسليح الثانوي نتج عنه تصرف مختلف تماما عن باقي العتبات حيث وجد عند زيادته يتغير نوع الفشل الى (فشل انحناء)، اما عند نقصان نسبة التسليح الثانوي يصبح نوع الفشل (انفصال في مستوى المفصل الانشائي).عند استخدام الاوتاد الكثيفة، كان لها تأثير على الليونة لأن الانحراف يقل، بينما استخدام عدد أقل من الاوتاد لم يكن له أي تأثير على سلوك العتبة. تم اعتماد بعض النتائج من الاختبارات التجريبية وتحليلها باستخدام تحليل العناصر المحددة (برنامج ANSYS) لدراسة تأثير استخدام الخرسانة عالية القوة ونسبة التسليح الثانوية على سلوك العتبات الخرسانية ذاتية الرص المسلحة. أشارت النتائج التحليلية إلى أن مقاومة القص للعتبات الخرسانية ذاتية الرص تزدادا مع زيادة قوة الخرسانة ونسبة حديد التسليح الثانوي. حيث أدى استخدام الخرسانة عالية المقاومة ٧٠ (نت/ملم٢) إلى ٤٧,٤٪ في الحمل الاقصى على القيمة التجريبية للخرسانة العادية ٢٨ (نت/ملم٢). وكذلك أدت زيادة نسبة التسليح الثانوي (٠,٠١٢٢٩ إلى ٠,٠٤٩) إلى زيادة مقدارها ١٠,٣٪ في مقدار الحمل الاقصى، بينما أدى تقليل نسبة التسليح الثانوي (٠,٠١٢٢٩ إلى ٠,٠٠٢٥) مع امتداد المسافة بين الاترية إلى تقليل مقدار الحمل الاقصى بمقدار ٥٥,٨ ٪.

الكلمات الدالة: الفواصل الانشائيه، الاوتاد (مسامير القص)، طريقة العناصر المحددة، خرسانة ذاتية الرص، تسليح ثانوي.

1.INTRODUCTION

Concrete may shrink or expand due to variations in temperature and moisture content; these changes result in movement, meaning that most concrete constructions need to have many joints of different kinds to keep the building's regular functions unhampered and to fit in with the building's general design [1]. Yousifani [2] Nonlinear three-dimensional finite elements were utilized to investigate the behavior of reinforced concrete beams with a Construction Joint (CJ). The parametric analysis took into account the kind of joint (horizontal or vertical), position, coefficient of friction at the contact, and proportion of steel in the joint. To investigate the aforementioned situations, two beams were introduced. They were evaluated in a number of places using either vertical or horizontal structural joints. Vertical joint effects were found to be negligible (the percentage loss in ultimate load capacity was between 0% and 10%), according to an analysis of the beams' behavior and load-carrying capacity. The overall performance and load-carrying capability of the structure were significantly impacted by the horizontal CJs (the percentage drop in ultimate load capacity ranged from 6% to 20%). Alghazali and Myers [3] experimentally studied the shear behavior of full-scale high-volume fly ash (HVFA-SCC) beams. Three alternative cement replacement levels were used in the beams' construction: 50%, 60%, and 70%. The findings indicated that, after 3 days, HVFA-SCC mixtures exhibited an early $f'c$ higher than 35 MPa. The shear strength capacity of HVFA-SCC beams with a low longitudinal reinforcement ratio (ρ=1.59%) was superior to conventional concrete (CC) beams. However, increasing the longitudinal reinforcement ratio unnoticeably affected the ultimate shear capacity; rather, it just delayed the development and propagation of a diagonal shear crack in HVFA-SCC beams. When the cement replacement level increased, the shear ductility of beams with shear reinforcement also increased. Shear ductility was increased by 35% when replacement levels were raised from 50% to 70%. The beam with 70% replacement had the highest shear ductility of the evaluated beams, even greater than the CC beam (between 7 and 35 % higher). In addition, it was noted that the HVFA-SCC beams with a 70% cement replacement level showed more deflection, cracking, and distribution than those with 50% and 60% cement replacement levels. Jabir et al. [4] experimentally examined the impact of CJ on the performance of reinforced concrete beams. Approximately 5% less beam strength was caused by the presence of a horizontal CJ at the tension zone. While inclined CJs negligibly affected the collapse load of the beams, ranging from 1.25% to 2.5%. Abbas et al. [5] examined the behavior of Reinforced Concrete (RC) beams when exposed to longitudinal CJ at various levels. The results revealed that the ultimate load, first crack load, and stiffness were all affected by the level of CJ. Ismael et al. [6] investigated the effect of CJ on the

structural performance of SCC beams. The study showed that the impact of the CJ on the ultimate load was greater than its effect on the first crack load. The horizontal joints were found to have a higher structural efficiency. Ibrahim et al. [7] performed an experimental study on RC beams that have no shear reinforcement to see the impact of CJ on shear capacity. According to the experimental program, the presence of a CJ substantially affected the shear behavior of the RC beam. The specimen with a vertical CJ at the mid-span showed a shear capacity reduction of up to 10%. The specimen with the interface perpendicular to the main shear crack significantly increased the shear strength by more than 30 %. Mathew and Nazeer [8] primary objective was to investigate the effect of CJ on the flexural attitude of RC beams. They examined the location and grade of these beams. The study showed that beams with a joint in the center one-third span had a slightly greater load-bearing capability than beams with a junction extending to the outer one-third span for the samples with concrete mixes (20MPa, 40MPa). Al-Rifaie et al. [9] examined the impact of the number and position of horizontal CJs (HCJs) on the flexural behavior of RC beams. Due to the presence of HCJs in reinforced concrete beams, the ultimate load was reduced, and ultimate deflection increased. Budi et al. [10] Investigated the shear behavior of high-volume fly ash-self-compacting concrete (HVFA-SCC) beams without stirrups, as well as whether the shear design code is appropriate for HVFA-SCC, given that the design code was established using knowledge from conventional concrete. Two types of HVFA-SCC beams measuring 100 mm × 150 mm × 1700 mm were manufactured utilizing 50% and 60% fly ash respectively. The 3D ATENA Engineering software was then utilized to numerically model the shear behavior seen in laboratory investigations. Numerical modeling was utilized to explore the effects of the a/d ratio, longitudinal reinforcement ratio (ρ), and beam depth. The results indicated that HVFA-SCC could be constructed using the ACI shear design code. Some of the previous studies examined the impact of construction joints on the mechanical characteristics of concrete; however, others examined shear interface capacity. Additionally, extensive research has been done on the type and position of construction joints, as well as the impact of surface treatment on CJ. It was noticed that although numerous studies examined the effect of construction joints in conventional concrete, only a few looked at SCC and UHPC because they are regarded as newly developed types of concrete. As a result, this research will examine many additional variables that influence the behavior of CJ in SCC beams, including joint location, compressive strength, flexural and stirrup reinforcement, and using dowels.

2.EXPERIMENTAL SCHEME

Twelve beams with dimensions of (150 ×180 ×1200) mm (width, height, and length) were cast and tested, one of which was cast monolithically (control specimen) (CB), and the others cast with a horizontal joint. The SCC mixture was mixed in two stages for all beams; the first part of each beam was poured to its structural CJ and left for 1 ½ to 2 hours (the time of the reaction of the cement with water and the loss of elasticity of cement). The specimens were painted white to demonstrate the development of the cracks during the testing procedure, as seen in Fig. 1. The variables examined in this study were CJ position, concrete $f'c$, variation in main reinforcement and secondary reinforcement, and dowel existence. Table 1 and Figs. 2 and 3 below display these details.

Table 1 Details of the Experimental Program.

Item	Groups	Designation	f'c (MPa)	Level of CJ	Vf *(mm)	Dowels	Main reinforcement
1	Reference	Control Beam CB	28	No joint	Ø4	No	3Ø12
2	G1	B1	28	Below N.A.	Ø4	No	3Ø12
3		B2	28	N.A.**	Ø4	No	3Ø12
4		B3	28	Above N.A.	Ø4	No	3Ø12
5	G2	B4	21	Below N.A.	Ø4	No	3Ø12
6		B5	47	Below N.A.	Ø4	No	3Ø12
7	G3	B6	28	Below N.A.	Ø4	No	3Ø16
8		B7	28	Below N.A.	Ø4	No	2Ø12
9	G4	B8	28	Below N.A.	Ø6	No	3Ø12
10		B9	28	Below N.A.	Ø2	No	3Ø12
11	G5	B10	28	Below N.A.	Ø4	dense	3Ø12
12		B11	28	Below N.A.	Ø4	light	3Ø12

*V_f: Secondary Reinforcement **N.A.: neutral axes.

Fig. 1 Preparing Molds, Casting, Curing and Coloring the Specimens.

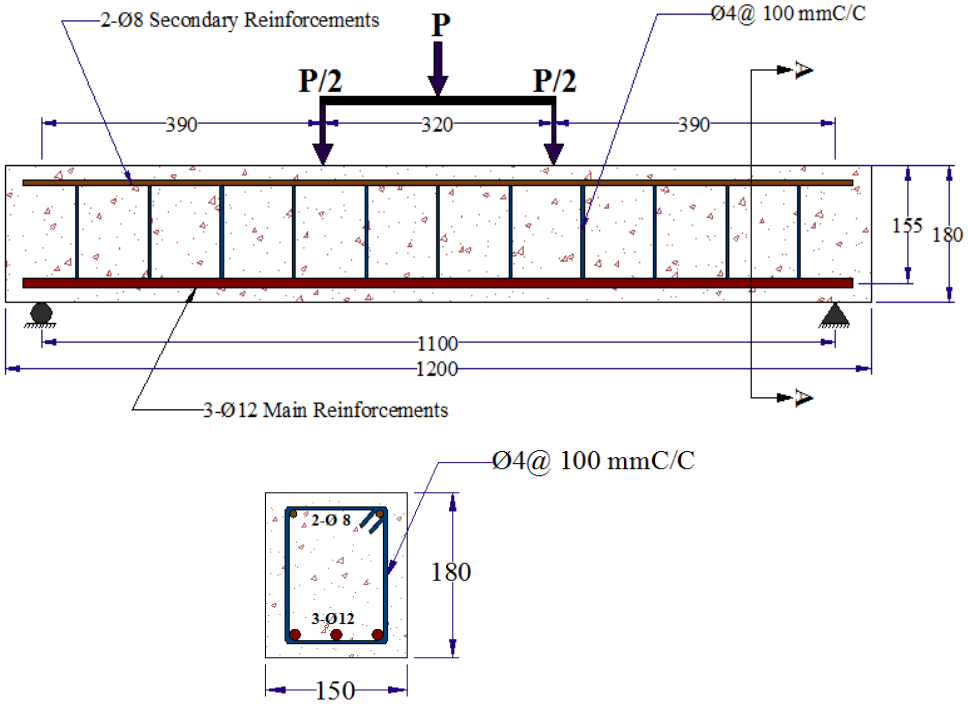

Fig. 2 Beam Details.

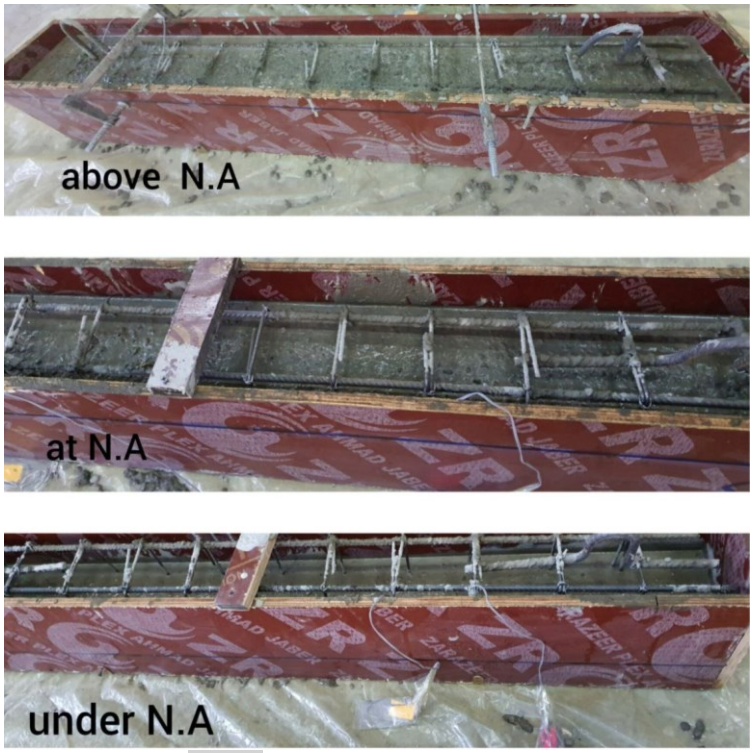

Fig. 3 Construction Joint Level.

To determine the strain on the steel bars, strain gauges of the type TML/ FLA-3-11-3L were employed. Three strain gauges were installed at three distinct places on each beam. Two were on the line connecting the load point to the support point (loading path), while the other was on the main bar reinforcement, as shown in Fig. 4. The slump flow and T50 cm and L-box tests were used to evaluate the SCC's capabilities according to EFNARC 2002 [11], as shown in Figs. 5 and 6.

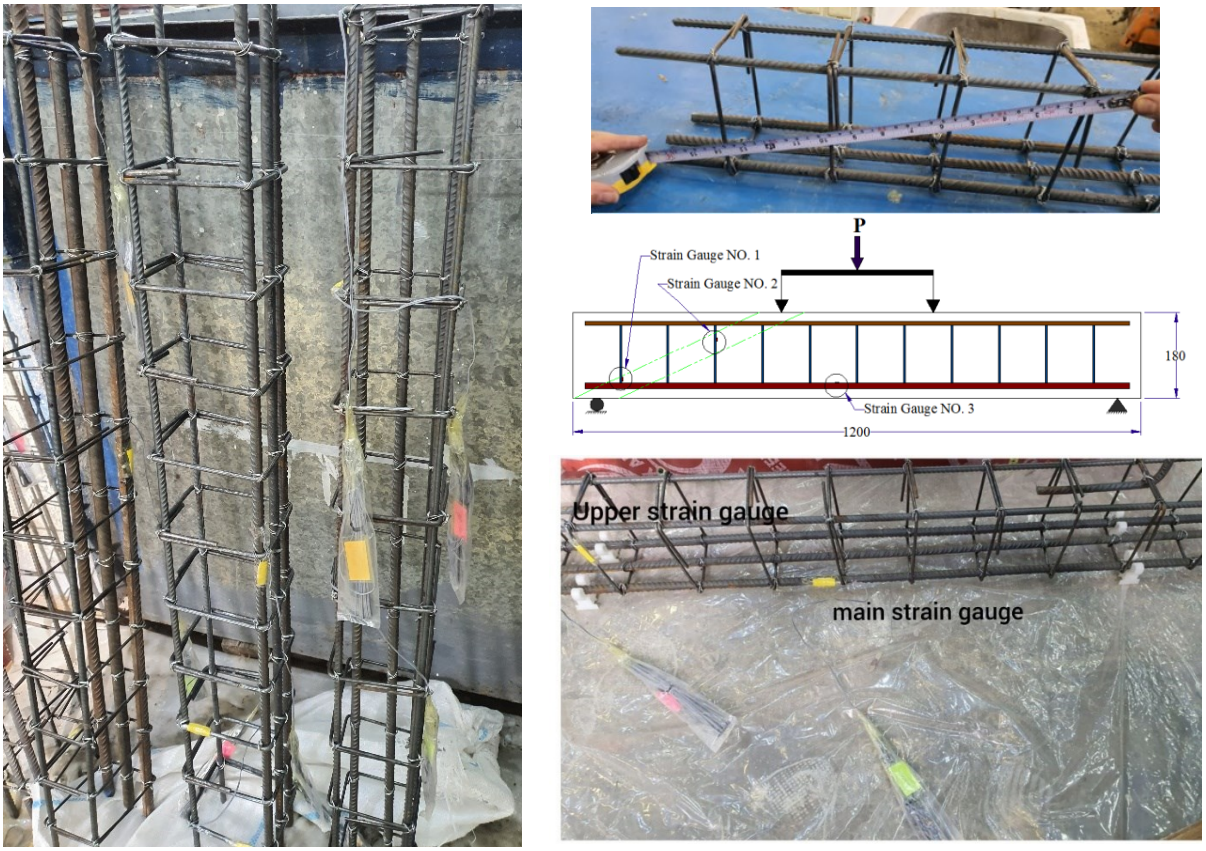

Fig. 4 Strain Gauge Position.

Fig. 5 Slump Flow Test.

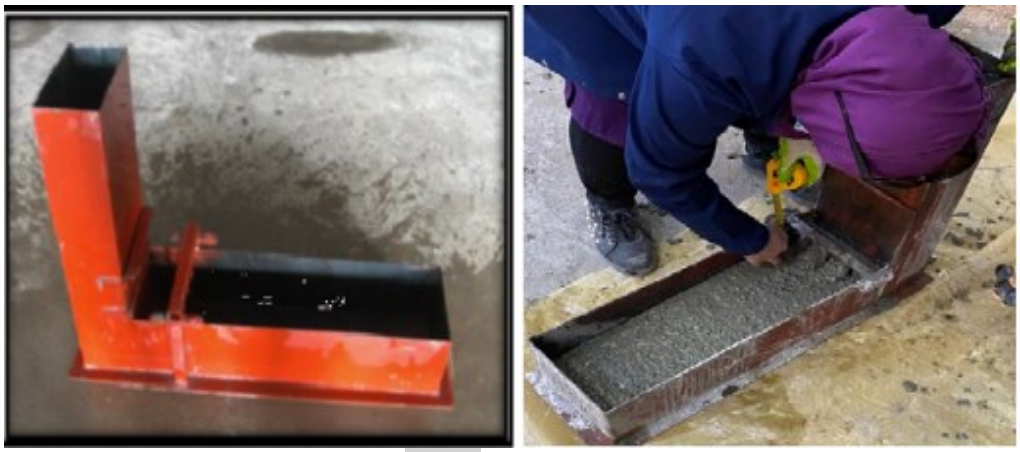

Fig. 6 L-box Test.

2.1.Test Setup

At Al-Nahrain University/Civil Engineering Laboratory, the beams were subjected to monotonic load/ two-point load testing utilizing a 2000 kN testing universal machine. Figure 7 shows the testing machine used in the test. The specimens were simply supported over an effective span length of 1100 mm and a loading distance of 390 mm from the support to obtain a share span to effective depth ratio of 2.6. Steel gauge wires were connected to the data logger, and the testing apparatus raised the load until it failed while continually recording the load and deflection.

Fig. 7 Testing Machine of 2000 kN.

2.2.Materials

Iraqi Standard Specifications No. 5, 1984, were met by using regular Portland cement (type I). [12]. Washed natural river sand with a fine modulus of (2.43) conforming to the requirements of the Iraqi Standard Specifications No.45, 1984 [13]. Gravel with a maximum size of 10 mm was utilized in the present study, fulfilling Iraqi standard No.45, 1984 [13]. A local limestone powder with a particle size of less than 0.125 mm was utilized to meet the EFNARC 2002 guideline [14]. GLENIUM 54, produced by (O. BASF), matches the criteria of ASTM C494/C494M-19 Type F& G [15], was used as a High Range Water Reducing Admixture (HRWRA). Tap water was utilized to mix and cure SCC specimens. In addition, 6 mm, 4 mm, and 2 mm plain bars were used as shearing reinforcement, and 8 mm deformed bars were used as nominal bars to support the stirrups. 16 mm and 12 mm deformed bars were used as the main flexural reinforcement, confirming the requirements of (ASTM A615/A615M-20) [16]. Reference SCC mixtures were proportioned according to references [17] and [18] to give a 28-day characteristic $f'c$. Table 2 displays the mixes used.

Table 2 Mix Proportions.

Mix NO.	f'c (MPa)	Cement (kg/m³)	Sand (kg/m³)	Gravel (kg/m³)	Limestone (kg/m³)	Water (l/m³)	HRWRA (l/m³)	Reference NO.
M1	21	250	983	766	139	195	4.6	15
M2	28	350	983	766	96	178	6.86	15
M3	47	474	758.4	833	105.3	180	5.7	16

2.3.Results of the Test

Almost all beam specimens displayed a similar pattern of failure, starting with a first flexural crack at around 34 to 54 percent of the ultimate load in the beam's mid-span (except for CB and B4, where the first crack was a shear crack). The deflections increased linearly as the loads increased. Almost all of the first shear fractures began at the CJ, and as the load increased, the primary cracks widened and spread upward and downward. While secondary flexural and shear cracks formed. Before reaching the failure load, the fracture patterns on the two sides of the beams were virtually identical. The beam collapsed when the major shear crack on one side of the beam reached the load and support points. Table 3 shows the results of testing all 12 SCC beams.

Table 3 Results and Failure Modes of SCC Beams.

Beam Desig.	Group	Variables	Crack Load Pcr (kN)	First crack type	Ultimate Load Pu (kN)	Pcr/Pult %	Maximum Deflection (mm)	Mode of Failure
Control		————	70	Shear	170	41.2	17.2	Diagonal Shear
B1	G1	Location of CJ	61	flexure	156	39.1	15.81	Diagonal Shear
B2			57	flexure	132	43.2	12.51	Diagonal Shear
B3			46	flexure	135	34.1	11.05	Diagonal Shear
B4	G2	Comp. Strength	78	Shear	90	86.7	10.60	Diagonal Shear
B5			61	flexure	162	37.6	15.90	Diagonal Shear
B6	G3	Main Reinf.	91	flexure	173	52.6	13.47	Diagonal Shear + Sliding in CJ
B7			64	flexure	115	53.04	9.38	Diagonal Shear + Sliding in CJ
B8	G4	Shear Reinf.	87	flexure	160	54.3	18.17	Flexural
B9			40	flexure	80	50	6.95	CJ sliding
B10	G5	Dowel's presence	34	flexure	165	20.6	12.16	Diagonal Shear
B11			45	flexure	158	28.5	15.04	Diagonal Shear

2.4.Load Deflection Curves and Crack Pattern

2.4.1.Control Beam

The control beam behaved elastically at low loads, with no cracks formation until the load reached 70 kN, at which point the first shear crack developed. Fractures developed and extended up to the point of tension zone. The load point was linked to a support point along the line of the major diagonal crack when the load reached 170 kN. Figure 8 shows the control beam's crack pattern and load-deflection curve.

2.4.2.Group 1: Location of CJ

The position of horizontal CJs affects the initial crack load more than the overall load, as shown in Table 4. As the level of construction joints rose away from the bottom of the beam, shear deformations decreased, as demonstrated by a narrower crack width. Because of the CJs, the beam's stiffness decreased, increasing deflection values. Referring to Fig. 9, B3, which has CJ within the compression zone, behaves similarly to CB.

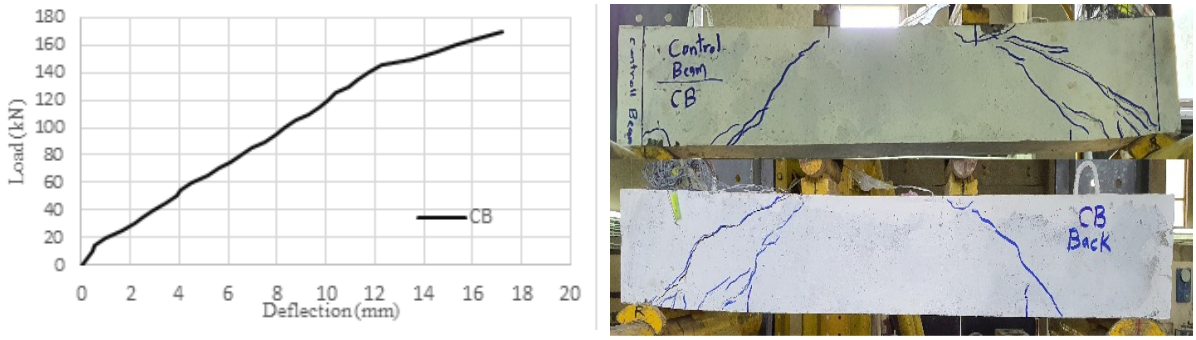

(a) **(b)**

Fig. 8 (a) Load-Deflection Curve for CB (b) Crack Pattern for CB.

Table 4 Results of Beams in Group 1.

Beam Designation	Location of CJ	*Pcr (kN)	**Var. %	***Pult (kN)	Var. %	Deflection (mm)
CB	_____	70	____	170	_____	17.2
B1	Low	61	-12.85	156	-8.2	15.81
B2	N.A.	57	-18.6	132	-22.4	12.51
B3	High	46	-34.3	135	-20.6	11.05

*P_{cr}=first crack load **Var. = variation ***P_{ult}=ultimate load

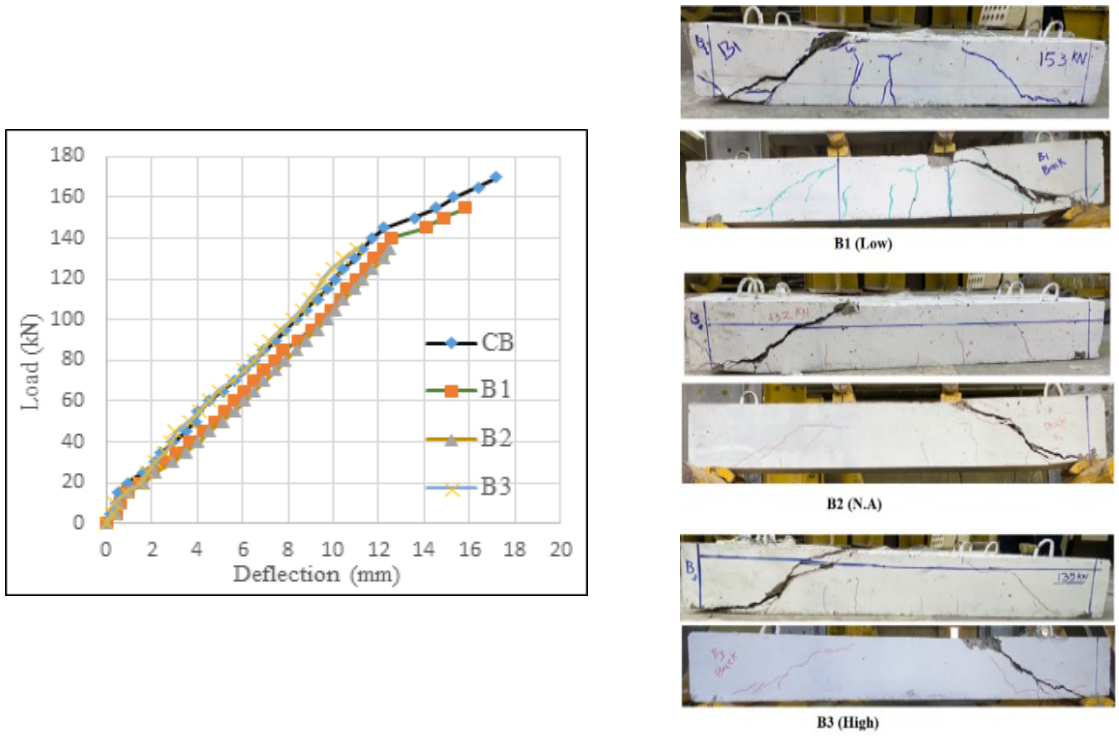

(a) **(b)**

Fig. 9 (a) Load Deflection Curve for Group 1 (b) Crack Pattern for Group 1.

2.4.3.Group 2: Compressive Strength (f'c)

Increasing the *f'c* of the concrete reduced deflection under the same applied load. Increased *f'c* significantly increased the modulus of elasticity, increasing flexure rigidity (EI), and increasing beam stiffness, significantly reducing deflection. From Table 5 below, it can be seen that decreasing *f'c* by (25%) resulted in a significant variation in the first and ultimate loads (27.8% and - 42.3%, respectively), whereas increasing *f'c* by (67.8%) insignificantly affected the first crack load. Figure 10 and Table 5 show these details.

Table 5 Results for Beams in Group 2.

Beam Designation	f'c (MPa)	Pc (kN)	Variation %	Pult (kN)	Variation %	Deflection (mm)
B1	28	61	------	156	-----	15.81
B4	21	78	27.8	90	- 42.3	10.60
B5	47	61	0	162	3.8	15.90

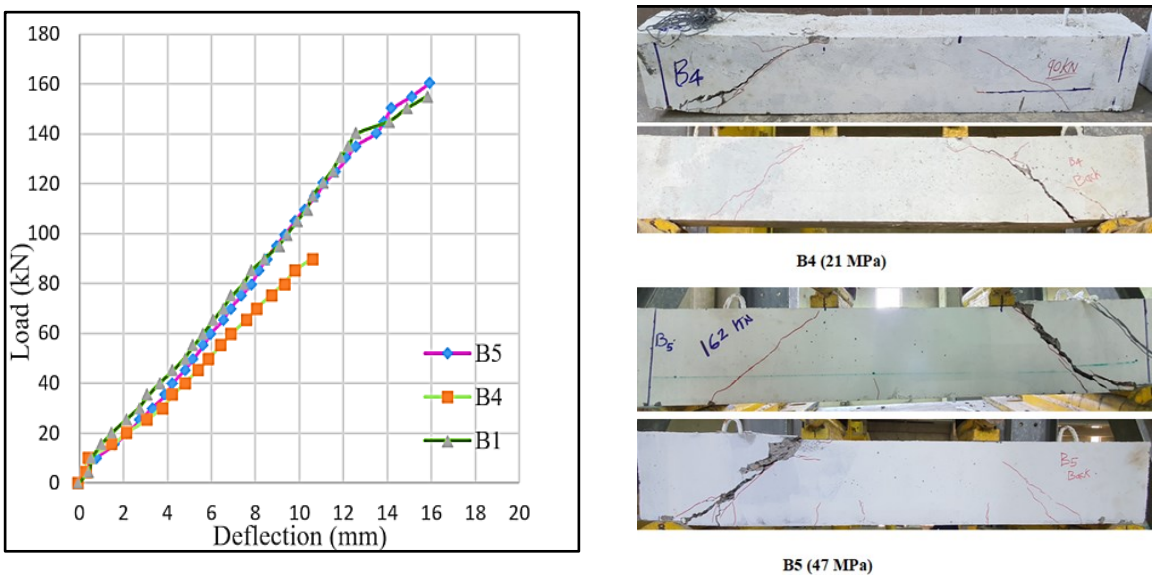

(a) **(b)**

Fig. 10 (a) Load Deflection Curve for Group 2 (b) Crack Pattern for Group 2.

2.4.4.Group 3: Amount of Main Reinforcement (ρ)

Changes in the reinforcement ratio noticeably affected the failure mode, as it changed to diagonal shear and CJ separation failure. Increasing the ratio of the main reinforcement of the reinforced concrete beam decreased the maximum deflection and because the concrete beam became less ductile as the main reinforcement was increased. Figure 11 displays the crack pattern and load-deflection curves. As illustrated in Table 6, increasing the main reinforcement ratio by 77.9% significantly affected first crack load and ultimate load by 49.2% and 9.8 %, respectively, whereas reducing the reinforcement ratio by 32.9% significantly affected ultimate load and deflection by - 26.3% and - 40.7%, respectively.

Table 6 Results of Beams in Group 3.

Beam Designation	Main Reinf. ρ	P_c (kN)	Variation %	P_{ult} (kN)	Variation %	Deflection (mm)
B1	0.01506	61	-----	156	-----	15.81
B6	0.0268	91	49.2	173	9.8	13.47
B7	0.0101	64	4.9	116	- 25.6	9.38

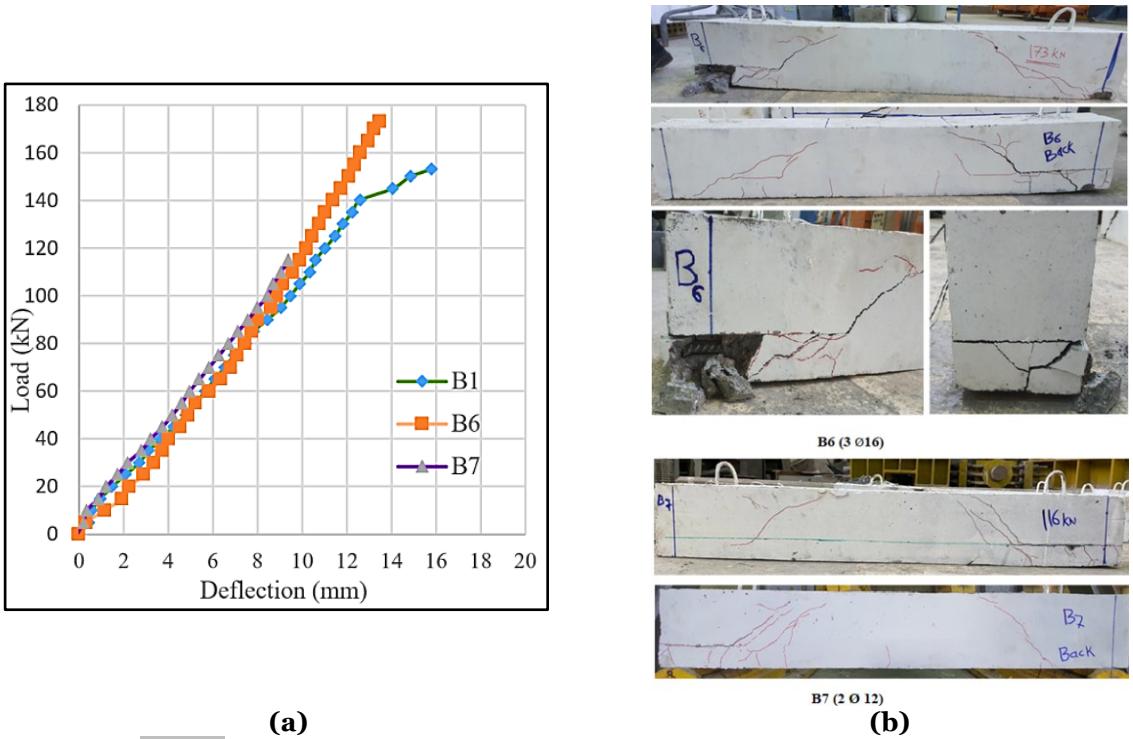

(a) **(b)**

Fig. 11 (a) Load Deflection Curve for Group 3 (b) Crack Pattern for Group 3.

2.4.5.Group 4: Amount of Secondary Reinforcement (ρv)

Figure 12 displays the crack pattern and the load-deflection curves for Group 4. It was noticed that when the ratio of secondary concrete reinforcement (shear reinforcement) was raised, the beam's maximum load exceeded B1, deflection decreased, and its failure mode was flexural as predicted after reinforcing the shear reinforcement, and that was expected as the shear reinforcement strengthening. While when the vertical reinforcement was reduced, the beam became more brittle, and failure (separation of the CJs) occurred soon after the first shear fracture developed. According to Table 7, increasing ρv by approximately (55.5%) increased the first crack load by 42.6% and the deflection by 14.9%, whereas decreasing ρv by 74.8% led to an influential decline in the first crack load, failure load, and deflection by 34.4%, 45.5%, and 56.04%, respectively.

Table 7 Results of Beams in Group 4.

Beam Designation	Secondary Reinf. ρ_v	P_c (kN)	Var. %	P_{ult} (kN)	Var. %	Deflection (mm)
B1	0.01229	61	-----	156	------	15.81
B8	0.0276	87	42.6	160	2.6	18.17
B9	0.0031	40	-34.4	80	- 48.7	6.95

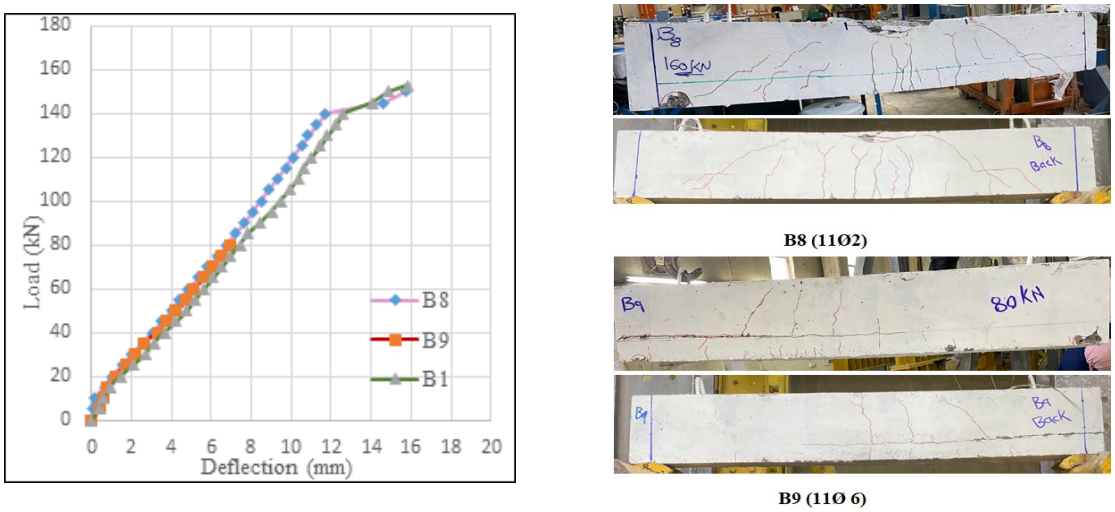

(a) **(b)**

Fig. 12 (a) Load Deflection Curve for Group 4 (b) Crack Pattern for Group 4.

2.4.6.Group 5: Dowels Existence (Shear/Steel Connectors)

As shown in Fig. 13 and Table 8, increasing the number of dowels (shear connections) stiffened the behavior and therefore decreased deflection values. Dense dowels significantly influenced the first crack load and deflection, decreasing both by (-44.3 % and 23.1%), respectively, while increasing the ultimate load by (5.8 %) because the interlocking mechanism between the concrete segments became more effective after adding the dowels, increasing the beam's load-bearing capacity. While adding light dowels insignificantly influenced the ultimate load behavior of the beam segments, it reduced the first fracture load (26.2 %).

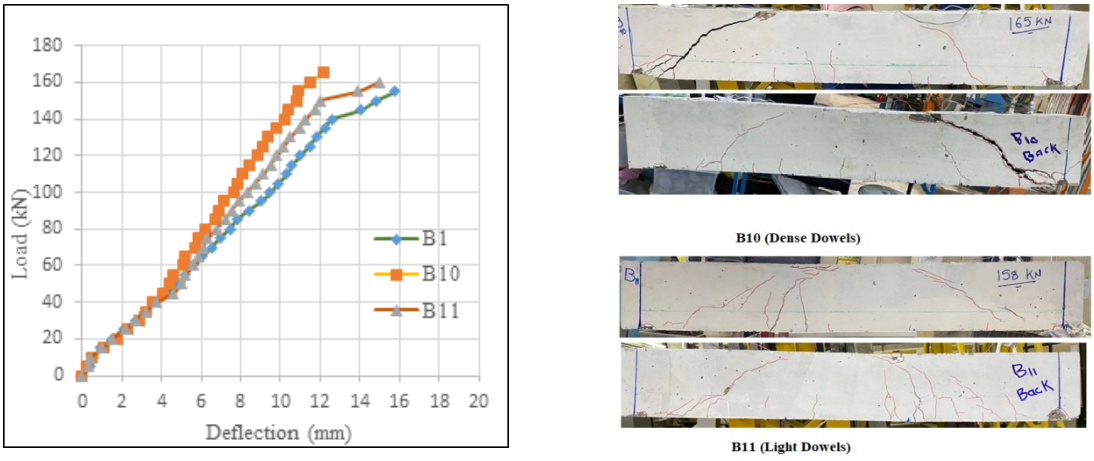

(a) (b)

Fig. 13 (a) Load Deflection Curve for Group 5 (b) Crack Pattern for Group 5

Table 8 Results of Beams in Group 5.

Beam Designation	Dowels	P_c (kN)	Var. %	P_{ult} (kN)	Var. %	Deflection (mm)
B1	No	61	-----	156	-----	15.81
B10	Dense	34	- 44.3	165	5.8	12.16
B11	Light	45	-26.2	158	1.3	15.04

2.5.Load-Strain Relationship

Strain gauges of the type TML/ FLA-3-11-3L were used to determine the strain on the steel bars. Three strain gauges were installed: two on the line connecting the load point and the support point and one on the main bar reinforcement. Steel gauge readings were taken every 5 kN from the start of the test until the failure. From the figures below, the following can be noticed:

- Figure 14: As the applied load increased in CB, the main and secondary reinforcement approached their yield points.
- Figures 15 and 16: Achieved their yielding points in the same manner as the CB, although at loads smaller than the CB load. Figure 17 shows that the secondary reinforcement did not reach its yield.
- Figures 18 and 19: When the concrete's $f'c$ was low, the main reinforcement achieved its yield point at a lower load than when the $f'c$ raised.
- Figures 20 and 21: Main and secondary reinforcement pass their yield points, while increasing main reinforcement had the opposite effect.
- Figures 22 and 23: Since B8 experienced strain but did not achieve its yield, adding the shear reinforcement improved the RC beam's shear capacity. B9 exhibited no yield when shear reinforcement was decreased, confirming the brittle failure at the CJ level of this beam.
- Figures 24 and 25: With dowels, the stirrups did not yield with dense dowels since the shearing capacity of the beam increased with the number of dowels used, while the main reinforcement exceeded its yield point. While utilizing light dowels insignificantly impacted shearing capacity since the stirrups' yield point was exceeded.

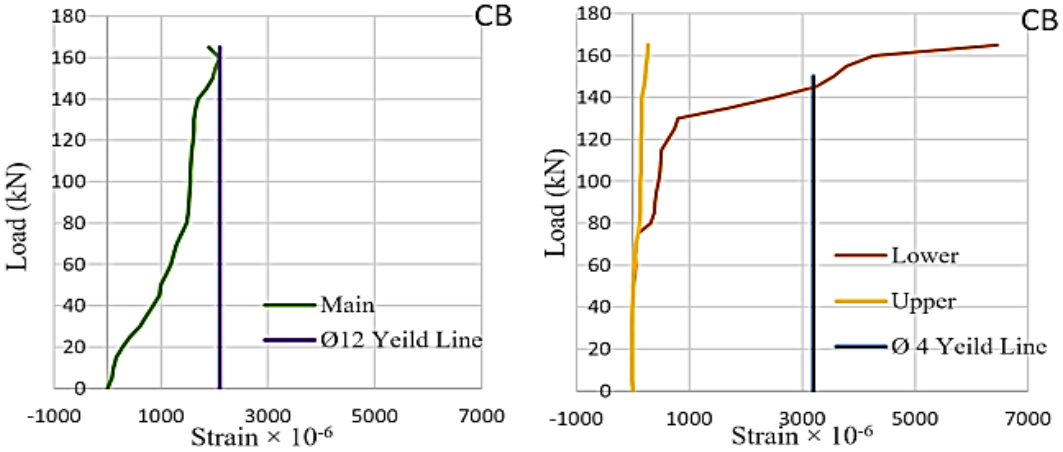

(a) ϕ12 mm main reinforcement **(b)** ϕ4 mm stirrups

Fig. 14 Load-Strain Relationships for CB.

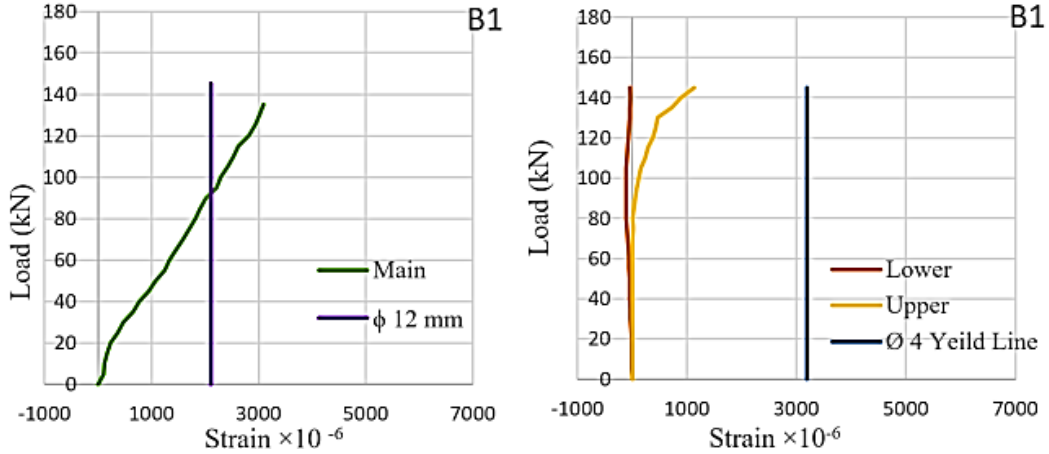

(a) ϕ12 mm main reinforcement **(b)** ϕ4 mm stirrups

Fig. 15 Load-Strain Relationships for B1.

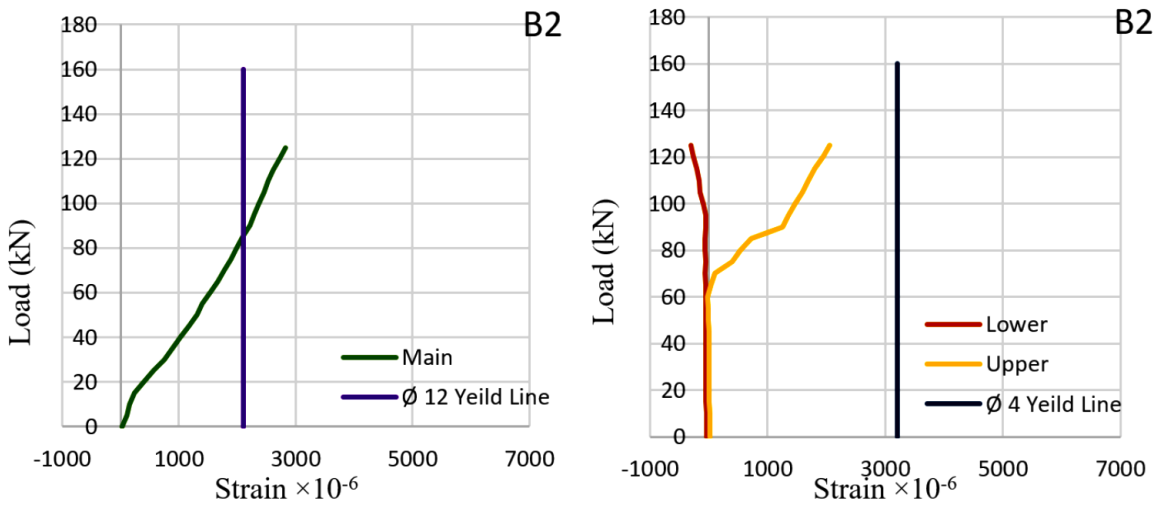

(a) ϕ12 mm main reinforcement **(b)** ϕ4 mm stirrups

Fig. 16 Load-Strain Relationships for B2.

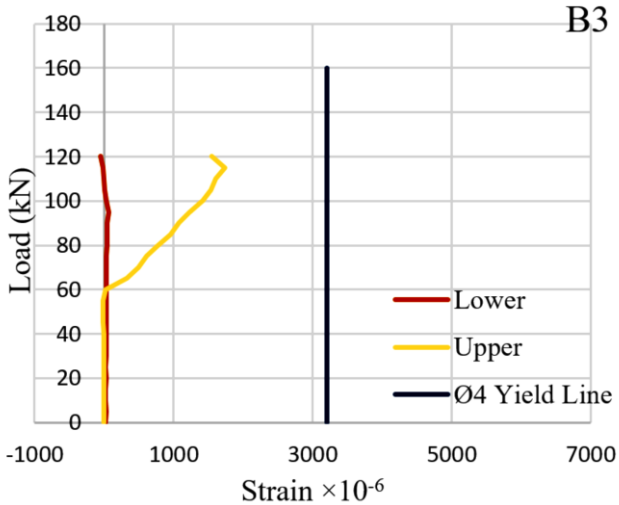

ϕ4 mm stirrups.

Fig. 17 Load-Strain Relationships for B3.

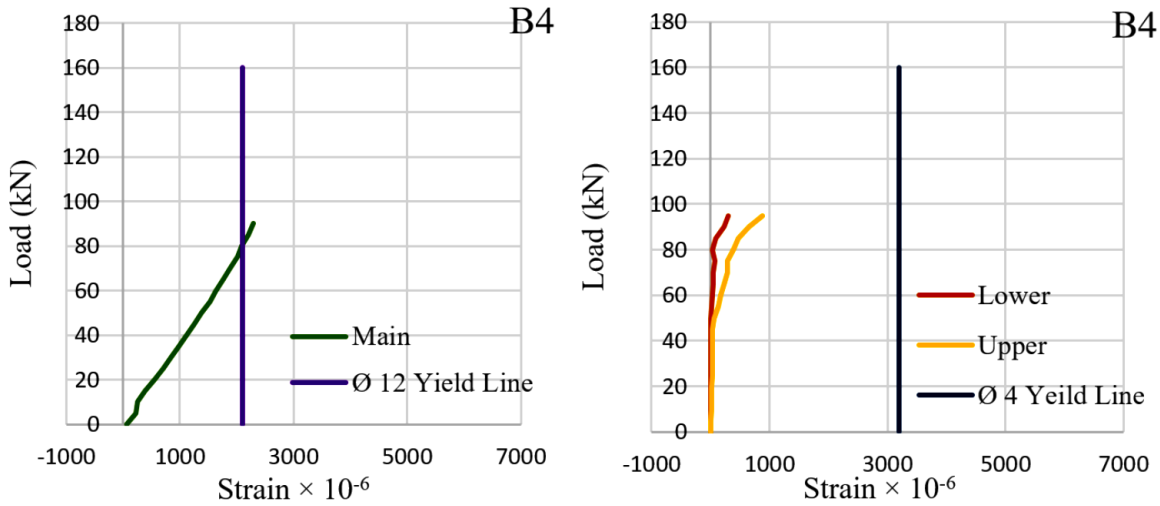

(a) ϕ12 mm Main Reinforcement. **(b)** ϕ4 mm Stirrups.

Fig. 18 Load-Strain Relationships for B4.

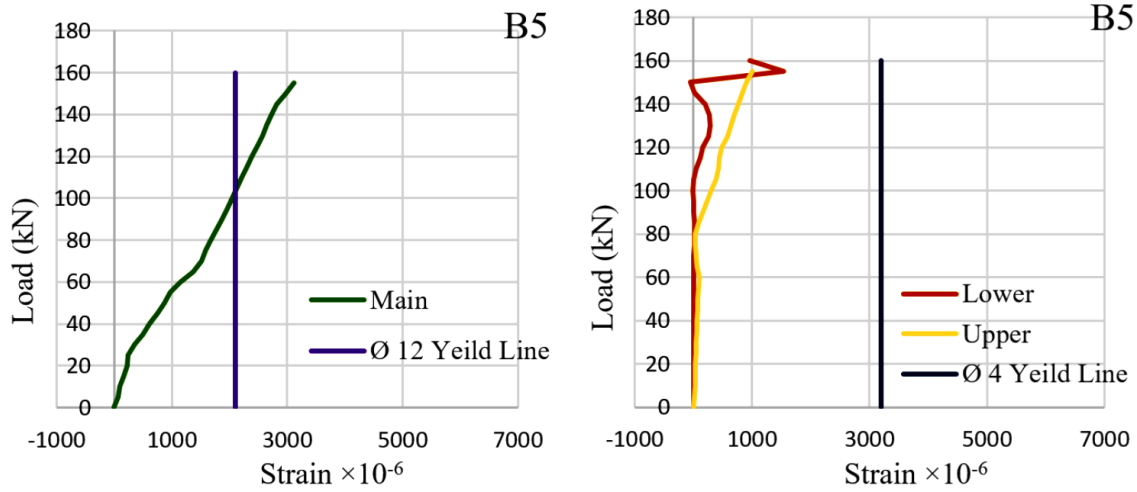

(a) ϕ12 mm Main Reinforcement. **(b)** ϕ4 mm Stirrups.

Fig. 19 Load-Strain Relationships for B5.

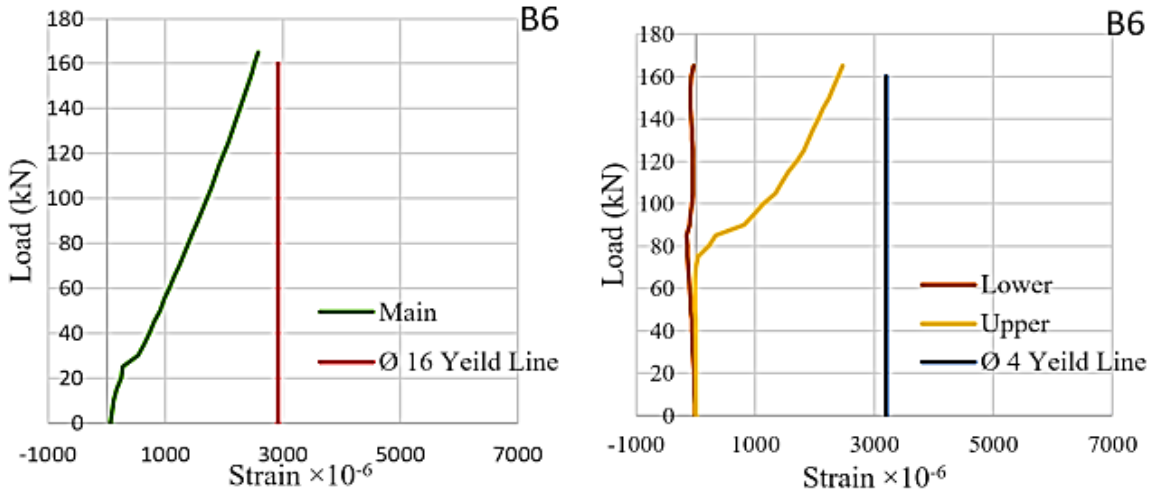

(a) ϕ16 mm Main Reinforcement. **(b)** ϕ4 mm Stirrups.

Fig. 20 Load-Strain Relationships for B6.

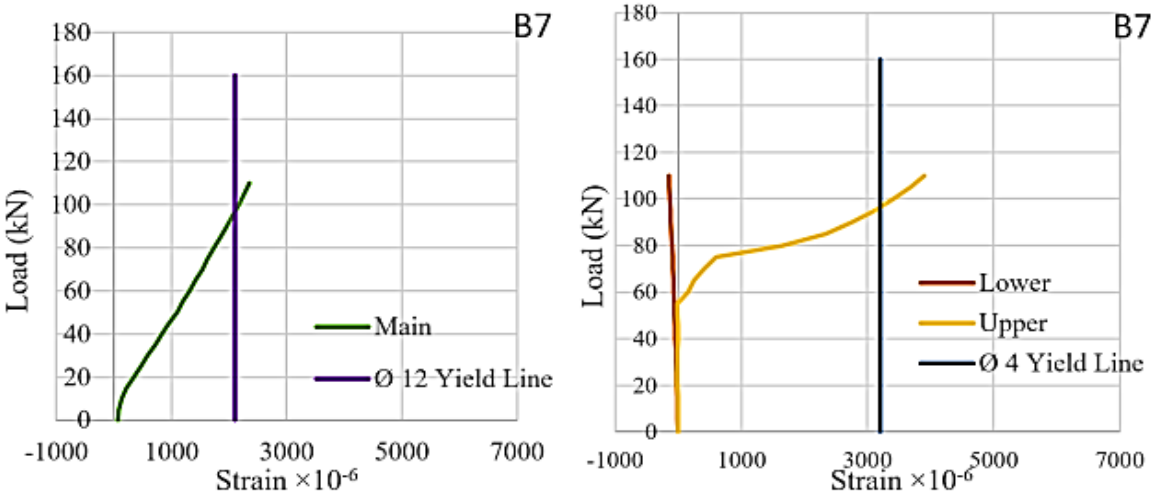

(a) ϕ12 mm Main Reinforcement. **(b)** ϕ4 mm Stirrups.

Fig. 21 Load-Strain Relationships for B7.

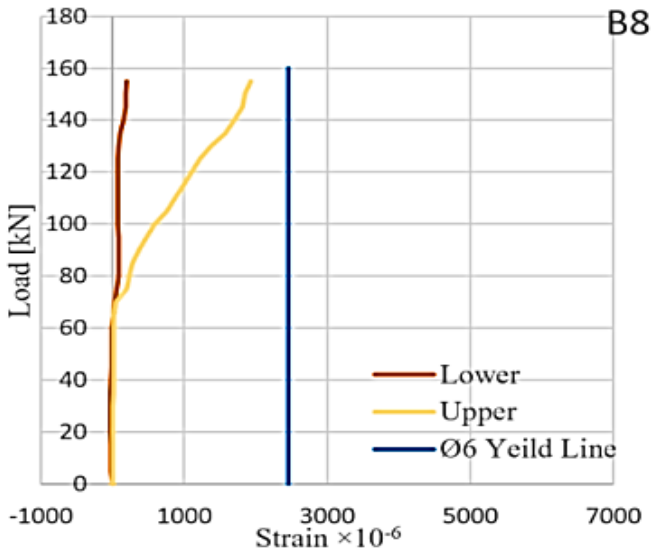

Φ6 mm stirrups.

Fig. 22 Load-Strain Relationships for B8.

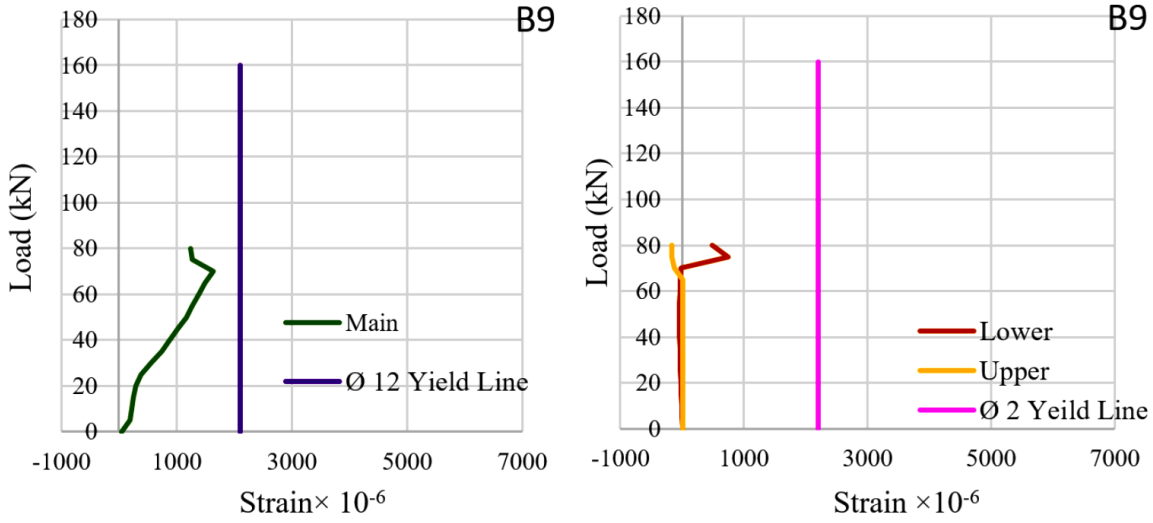

(a) ϕ12 mm Main Reinforcement. **(b)** ϕ4 mm Stirrups.

Fig. 23 Load-Strain Relationships for B9.

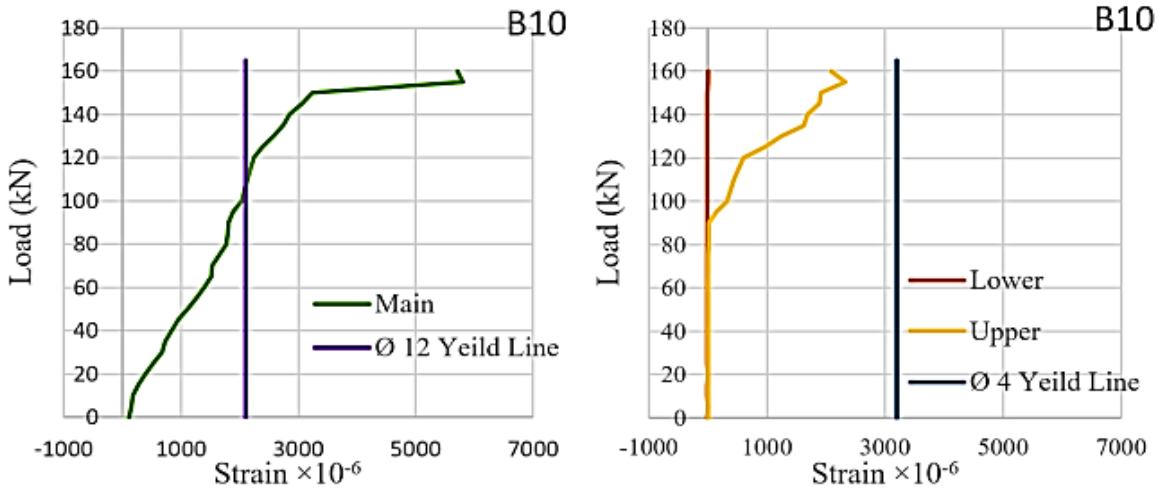

(a) ϕ12 mm Main Reinforcement. **(b)** ϕ4 mm Stirrups.

Fig. 24 Load-Strain Relationships for B10.

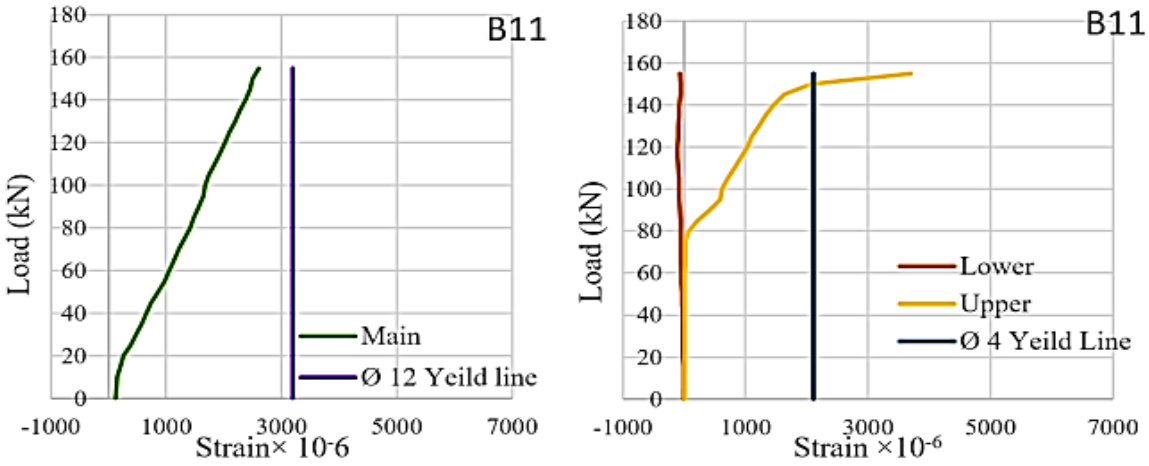

(a) ϕ12 mm Main Reinforcement. **(b)** ϕ4 mm Stirrups.

Fig. 25 Load-Strain Relationships for B11.

3.THEORETICAL STUDY

3.1.Loading and Support Steel Plates Modeling

Steel plates were added to the loading and support sites' finite element models to prevent local failure and stress concentration. The solid 45 was used to represent structural components in 3D. The element's eight nodes each have three degrees of freedom, allowing for translation in the nodal x, y, and z directions. The element's properties include plasticity, creep swelling, stress stiffening, large deflection, and large strain [18]. The form, node locations, and coordinate system of this element are shown in Fig. 26. The dimensions of the plates used in this study were (50 mm wide, 150 mm long, and 40 mm thick). Figures 27 to 29 display the boundary and loading conditions and reinforcement at CB.

3.2.Horizontal Construction Joint Modeling (Interface Modeling)

An interface connects two different types of concrete. Under these conditions, assuming the monolithic behavior of the final composite reinforced concrete components is strongly reliant on the concept of concrete-to-concrete interface load transfer. It is crucial to investigate how three forces—tension, compression, and shear—are transmitted [19]. According to Randl [20], While external tensile stresses are transported over the interface by reinforcing, compression forces pass directly through the concrete. Ensuring that shear forces are dispersed throughout the joint is the main goal. Terms like mechanical interlock, adhesive bonding, friction, or dowel action might be used to define the contact shear transfer technique. This study used two sets of interface models to model interface interaction. The first interface can endure tangential shear (Coulomb friction) as well as compression forces normal to the contact surface. TAUMAX is the greatest contact friction stress that may be given without causing sliding, regardless of the normal contact pressure used. Based on Ref's findings, TAUMAX = √fc' MPa was used for this study. [17]. This interface model was idealized using the CONTA172 and TARGE169 two-dimensional surface-to-surface contact elements.

3.2.1.CONTA172

CONTA172 specifies the contact and sliding between two-dimensional target surfaces (TARGE169) and a deformable surface. The element may be utilized in studies of two-dimensional structural and coupled-field contacts. It is appropriate for pair-based and general interaction. In the case of pair-based contact, The type TARGE169 was a 2-D target element that defined the target surface. Either TARGE169 elements (for rigid bodies only) or CONTA172 elements (for deformable surfaces) can be used to identify the target surface in the case of general contact. An element surface makes contact when it passes through a corresponding target surface and displays the same geometric characteristics as the solid element face it is attached to. Supported friction types include coulomb friction, shear stress friction, user-defined friction using the USERFRIC subroutine, and user-defined contact interaction with the USERINTER function. Additionally, this component permits the separation of bonded contacts, simulating interface delamination. [18]. Figure 30 shows its geometry, and Fig. 31 displays the interface layer used in B1 (beam with HCJ at tension zone).

3.2.2.TARGE169

TARGE169 represents several two-dimensional "target" surfaces for the related contact components (CONTA171, CONTA172, and

CONTA175). The contact elements may come into contact with TARGE169 or the target surface, and they are located on the solid elements that define the boundary of a deformable body. The target segment element may be subjected to translational or rotational displacement, voltage, magnetic potential, temperature, pressure, or moments [17]. Figure 32 depicts the geometry of TARGE169.

3.3.Numerical Integration and Nonlinear Solution Procedures

This study used the Gauss quadrature approach to calculate the integrals required to set up the element stiffness matrix. The integration rule used in this work is 8 (2×2×2) points Fig. 33. The locations of the sampling points and the weighting factors for the 2×2×2 integration rule is shown in Table 9. The Newton-Raphson algorithm and incremental-iterative solution techniques were used by the ANSYS application. As shown in Fig. 34, Iterations are performed to establish a converged solution that corresponds to the loading stage in question, while the load is applied incrementally.

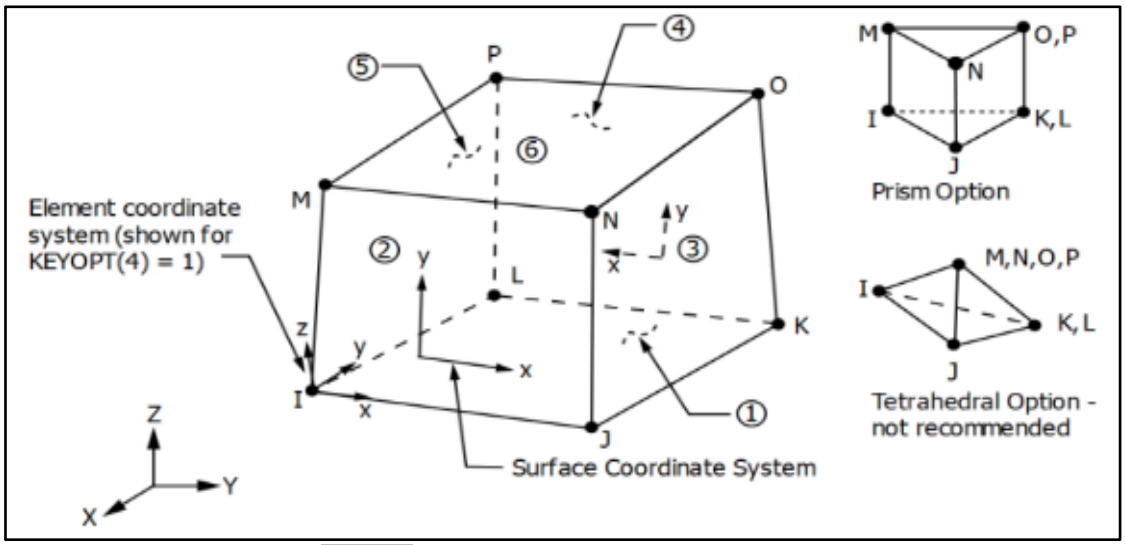

Fig. 26 Solid 45 Element Geometry [18].

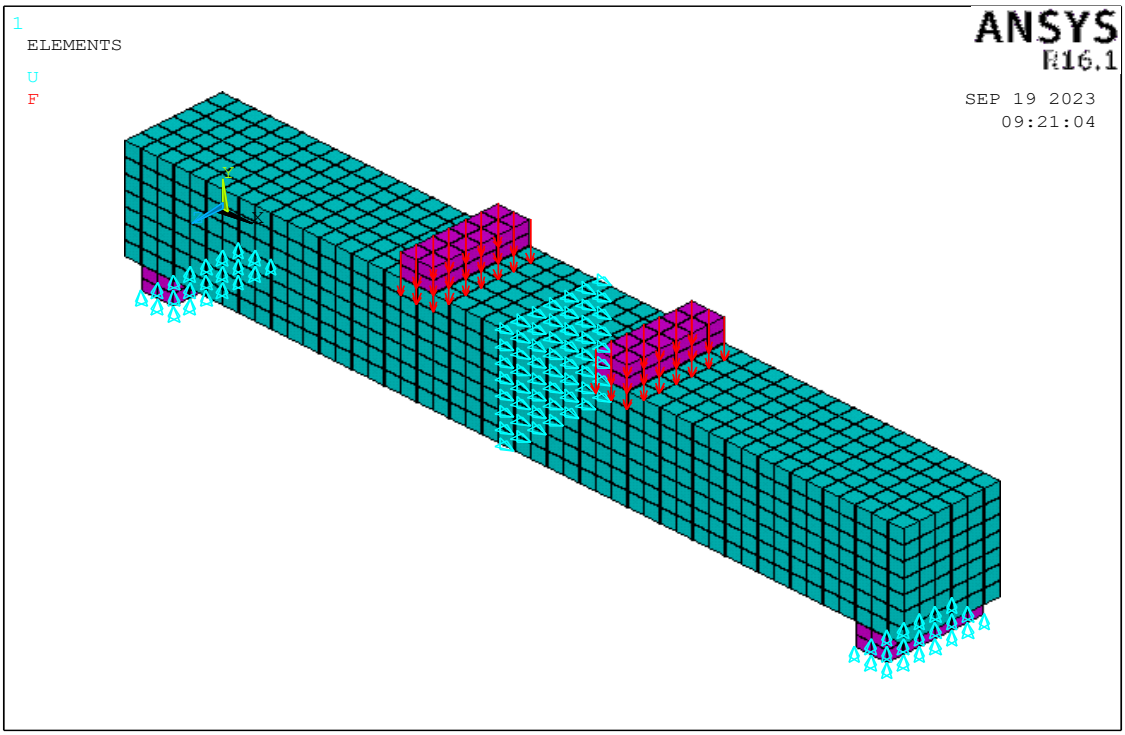

Fig. 27 CB Loading and Boundary Conditions Plates.

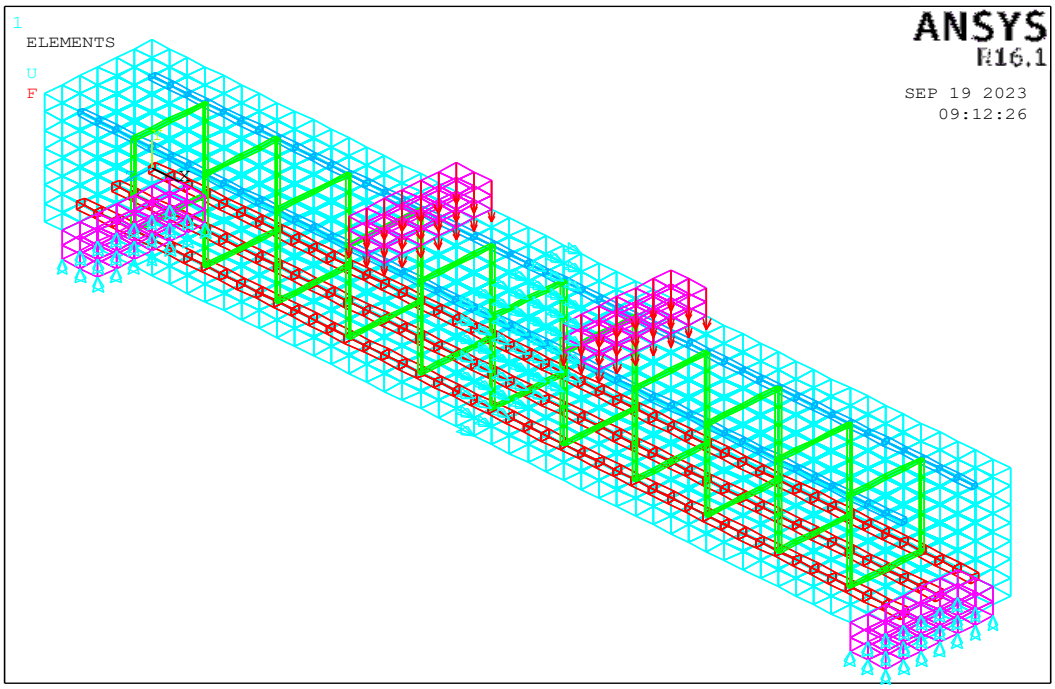

Fig. 28 Steel Reinforcement at CB.

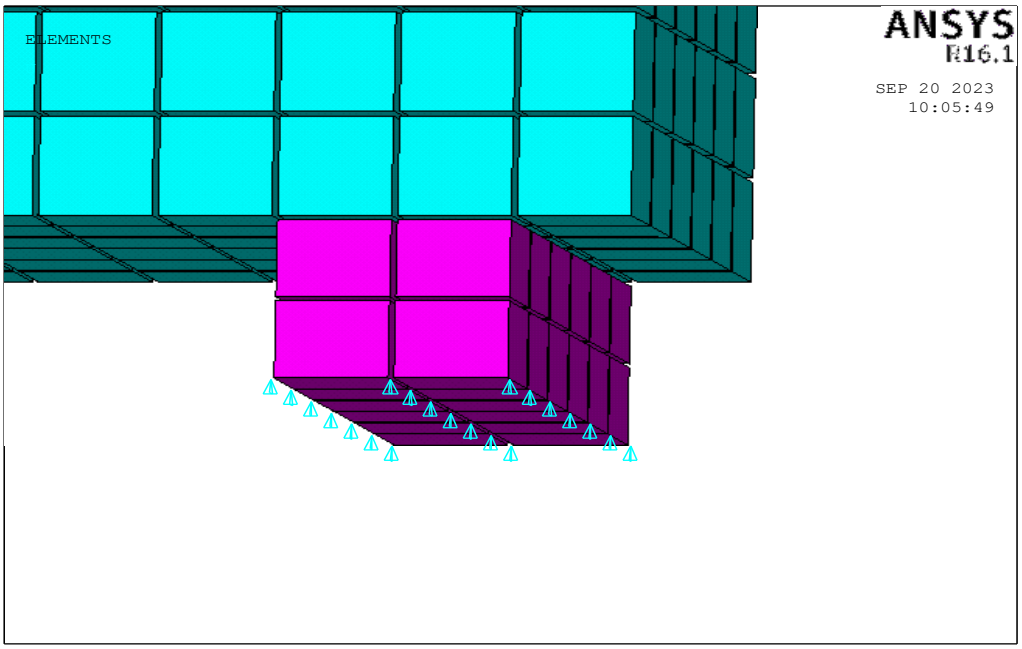

Fig. 29 Boundary Conditions (Simply Supported).

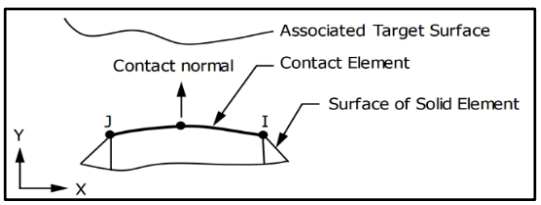

Fig. 30 CONTA172 Element [18].

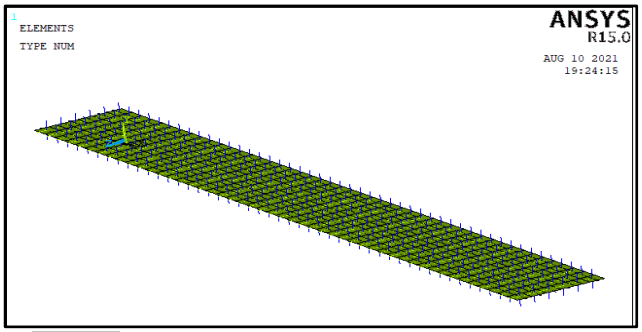

Fig. 31 B1 Interface (HCJ) Modeling in ANSYS.

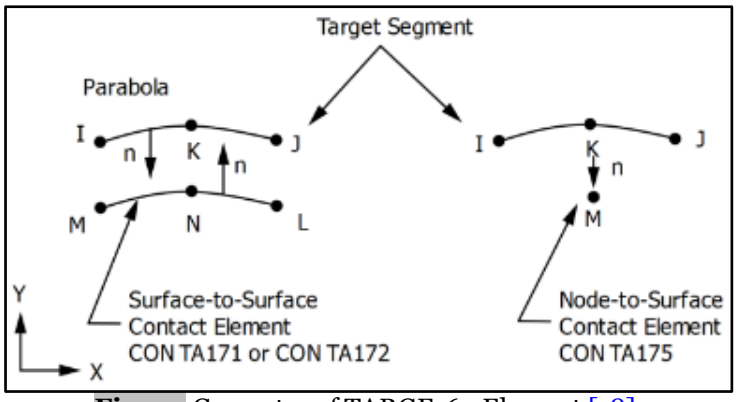

Fig. 32 Geometry of TARGE169 Element [18].

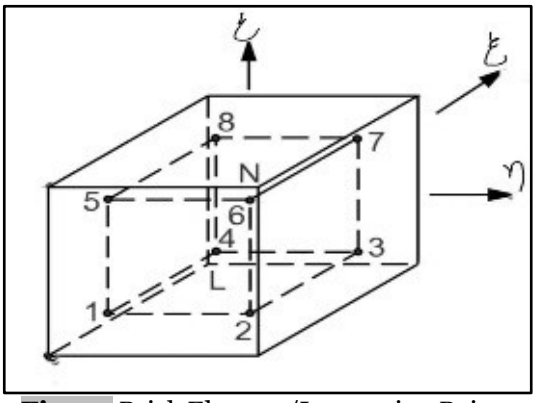

Fig. 33 Brick Element/Integration Points Location [18].

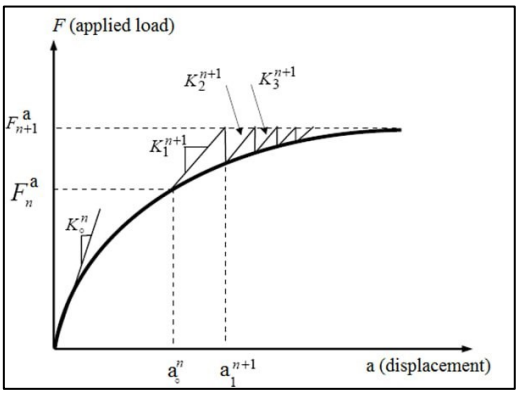

Fig. 34 Incremental-Iterative Method [18].

Table 9 Sampling Points Position and Weighting Factor for 2× 2× 2 Gauss Quadrature [18, 21].

Sampling Point	Position of points			Weight
	ξ	η	ζ	
1-8	± 0.57734	± 0.57734	± 0.57734	1

3.4.Finite Element Results

3.4.1.Load and Deflection at Failure

Figure 35 shows the ultimate load and failure deflection of the control beam as established by finite element analysis (ANSYS). The CB and B1 had respective FEA loads of 161 and 145 kN at failure. On the other hand, the experiment's failure load was 170 kN and 156 kN, respectively, meaning that there was a failure load differential of roughly 5.6%. Figures 36 and 37 show the experimental and analytical load-deflection curves for the control beam and B1 (CJ at the tension zone). HCJ caused the beam to become less stiff, as seen in Fig. 38.

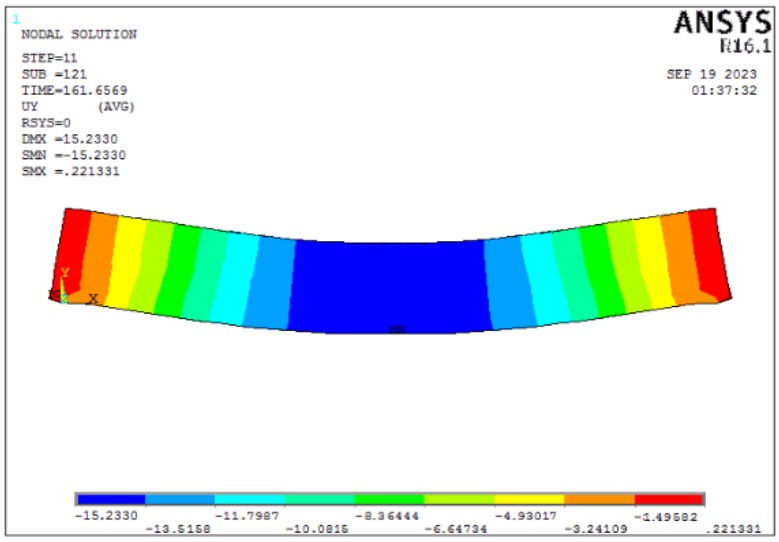

Fig. 35 Failure Load and Deflection for CB.

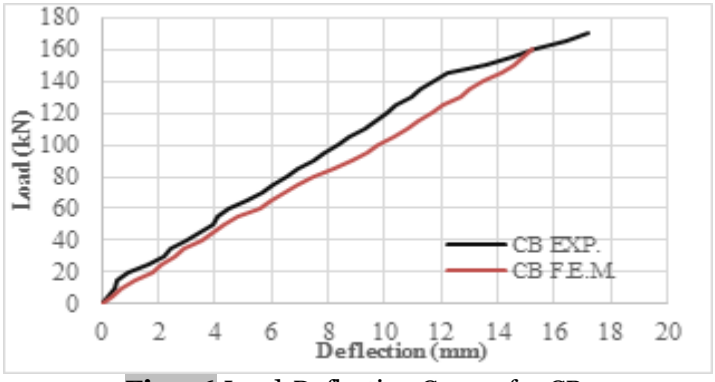

Fig. 36 Load-Deflection Curves for CB.

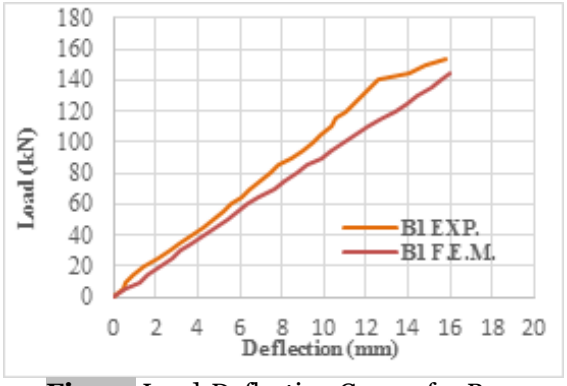

Fig. 37 Load-Deflection Curves for B1.

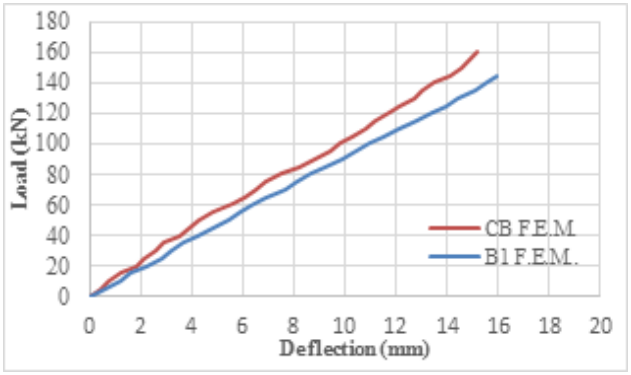

Fig. 38 Load-Deflection Curves for CB and B1.

3.4.2.Crack Patterns

Cracking or crushing fractures in concrete components are represented by circles placed at sample locations in the ANSYS computer program. The following categories apply to crack and crush fractures:

1- Cracking is shown by a circular shape in the fracture plane.
2- Crushing is represented by an octahedron.
3- An X will be put over the corresponding circle of the circular contour if a fracture has been opened and then closed.

The integration point of each brick piece may break into three distinct planes. The first crack is labeled with a red circle outline, the second with a green circle outline, and the third with a blue circle outline. [17]. The fracture pattern of the control beam at the ultimate analytical load (163 kN) is shown in Fig. 39.

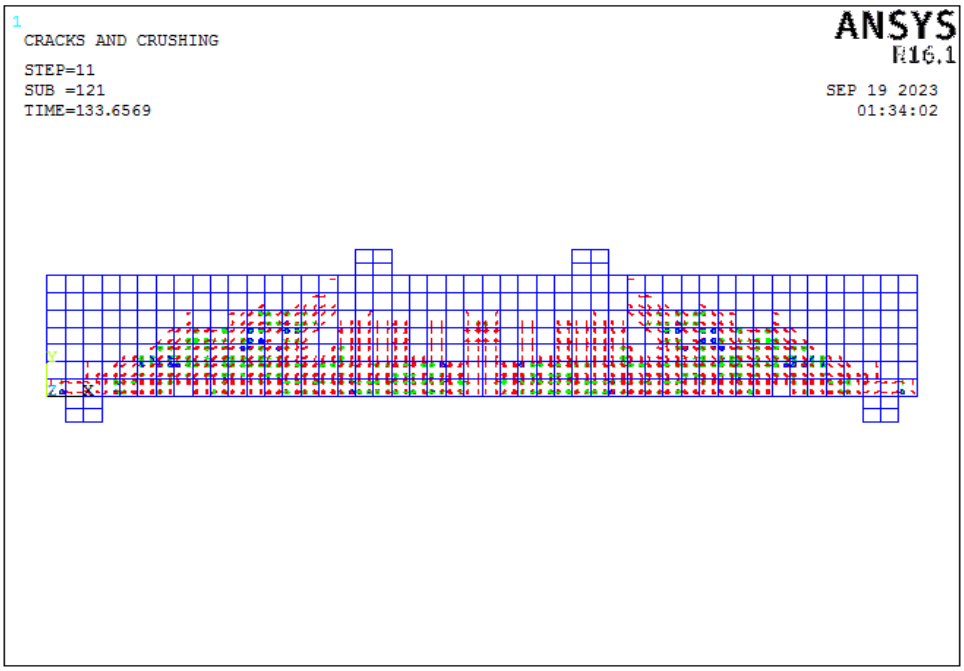

Fig. 39 CB Cracks Pattern in FEA at Ultimate Load.

3.4.3.Stress Distribution for Concrete

The distribution of concrete stress for CB at the ultimate load is shown in Fig. 40. At mid-span, when the top fibers of the cross-section are under compression, and the bottom fibers are under tension, the higher compressive stresses are clearly apparent. The compressive stress with the greatest value recorded (-29.63 MPa) was directly under the applied load.

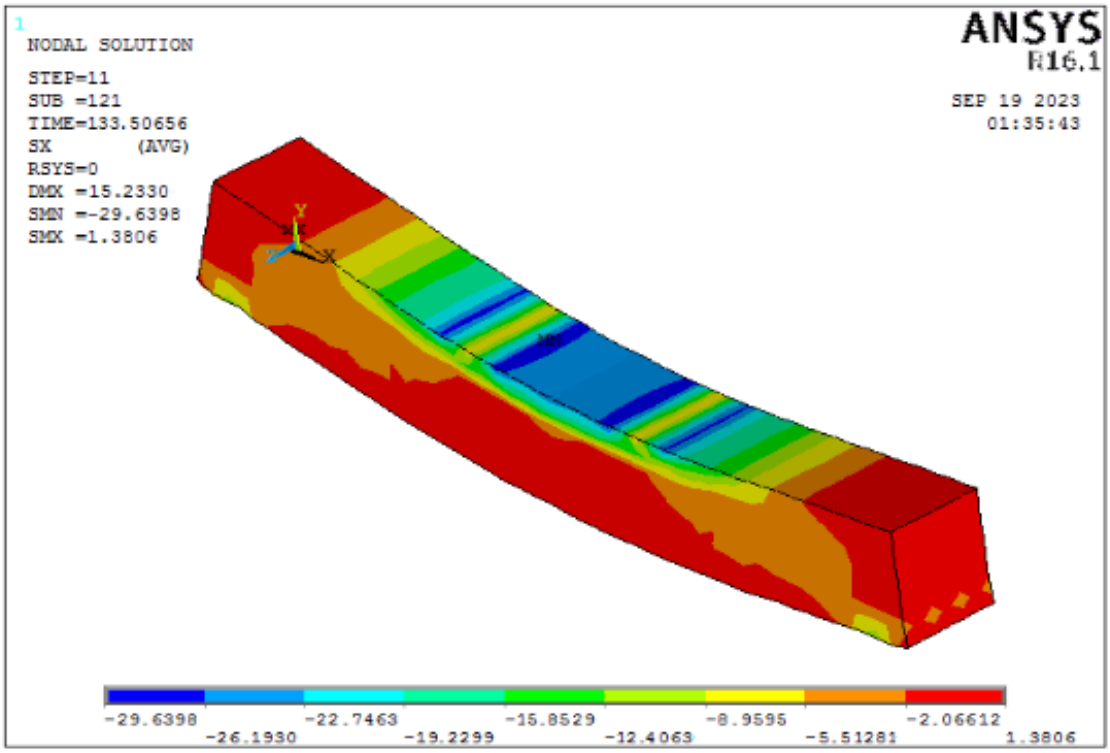

Fig. 40 Stress Distribution in Concrete for CB at Ultimate Load.

3.4.4.Stresses in Steel Reinforcement

Strain gauges were put on the steel reinforcing bars to monitor stress for the experimental program. However, virtual strain (and stress) gauges constructed using finite element analysis could eliminate the time-consuming process of measuring stress distribution along steel bars. Steel stresses in four stirrups (from right) of a control beam between the applied load and the support area are shown in Figs. 41 and 42. The yield stress of the 4 mm stirrups used in CB was (640 MPa), indicating that all the stirrups have yet to reach their yield point. The maximum stress measured in the middle stirrups (3rd) between load and support was about 440 MPa. Noticing that during the experiment, the stirrups' yield point was exceeded.

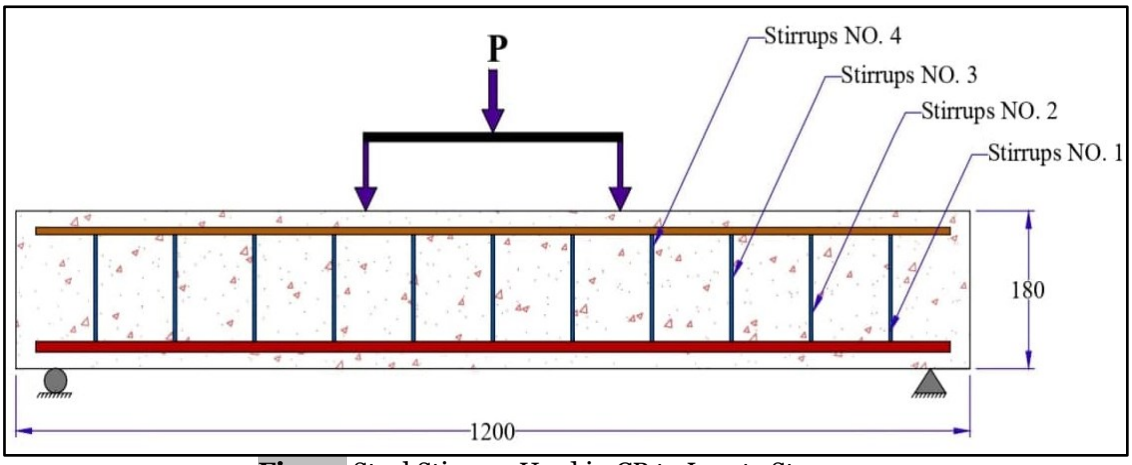

Fig. 41 Steel Stirrups Used in CB to Locate Stresses.

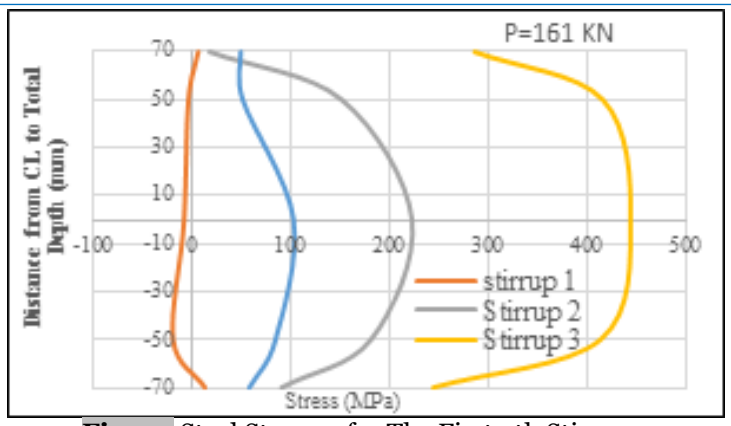

Fig. 42 Steel Stresses for The First 4th Stirrups.

3.4.5.Parametric Study for Experimental Data

The beam designated as (B1) studied in the preceding article was chosen for parametric study to determine the various material and solution variables' effect on the reinforced SCC beams' behavior in the presence of CJ. The impact of concrete *f'c* and stirrup reinforcement was considered.

a. Effect of Concrete Compressive Strength (f'c)

The concrete's *f'c* values for beam B1 in this investigation were 21, 28, 47, and 70 MPa. The ultimate burden rises in tandem with *f'c*. Comparing the analyzed beam to the experimental B1, Table 10 shows the numerical ultimate loads attained for different concrete grades.

Table 10 Effect of Grade of Concrete at the Ultimate Load of B1.

Value of (f'c) (MPa)		Numerical ultimate load (kN)	Pult/Num../ Pult/FEM *	Pult/Num../ Pult/Exp. **
B1	21	79	0.54	0.51
	28	145	1	0.93
	47	158	1.09	1.01
	70	230	1.59	1.47

* P_{ult} FEM = 145 kN (*f'c*=28 MPa) **$P_{ult/exp}$ = 156 kN (*f'c*= 28 MPa)

b. Effect of Stirrup Reinforcement

In this research, the secondary reinforcement (stirrups) ratios for B1 were 0.0025, 0.0031, 0.01229, 0.0276, and 0.049 at *f'c* 28 MPa. The ultimate load clearly increased as the secondary reinforcement ratio of concrete increased. Table 11 illustrates the numerical ultimate loads computed for various secondary reinforcement ratios for concrete in the analyzed beam to the experimental B1.

Table 11 Effect of Secondary Reinforcement Ratio at Ultimate Load of B1.

Value of ρv		Numerical ultimate load (kN)	Pult/Num../ Pult/FEM *	Pult/Num../ Pult/Exp. **
B1	0.0025	69	0.46	0.44
	0.0031	74	0.49	0.47
	0.01229	150	1	0.96
	0.0276	155	1.03	0.99
	0.049	172	1.15	1.1

* P_{ult} FEM = 145 kN (*f'c*=28 MPa). **$P_{ult/exp}$ = 156 kN (*f'c*= 28 MPa).

4.CONCLUSION AND DISCUSSION

The primary goal of this study is to determine how CJs affect the shear behavior of reinforced SCC beams at the joint regions.

4.1.Experimental Study

Twelve beams were divided into five groups, each group specializing in a single variable, and the following conclusions were drawn based on the results of the tests:

1- Location of CJ:

The existence of the CJ reduced the stiffness of the beam, resulting in greater deflection values; however, the maximum deflection of the CB remained greater. Due to its proximity to the CB, the CJ should be placed in the compression zone.

2- Compressive Strength (*f'c*):

Increasing *f'c* by (67.8%) insignificantly affected the initial crack load because it remained constant; however, it decreased deflection due to the fact that increasing *f'c* leads to a significant rise in modulus of elasticity, increasing flexure rigidity (EI), and that increased the beam stiffness, which significantly lowers deflection. While decreasing f'c by (25 %), deflection increased at the same applied load. Reducing *f'c* resulted in a substantial

difference in the first and ultimate loads by 27.8 % and - 42.3%, respectively.

3- **Main Reinforcement (ρ):**
When flexural reinforcement changes, the failure mode will often transition to separating the CJ Level + diagonal Shear Failure. Increasing the bending reinforcement ratio by 77.9% substantially impacted the first crack load, ultimate load, and deflection by 49.2%, 9.8 %, and - 14.8%, respectively. The concrete beam became less ductile as the main reinforcement increased. While reducing the bending reinforcement ratio by 32.9 % had a major effect on ultimate load and deflection, with - 26.3 % and - 40.7 %.

4- **Secondary Reinforcement (ρ_v):**
Secondary reinforcement substantially impacted the beams' behavior as the failure mechanism of the beams was significantly different from the others. Increasing ρv by approximately (55.5%) increased the first crack load by 42.6% and the deflection by 14.9%, and the failure mechanism turned into flexural failure. Decreasing ρv by 74.8% influentially declined the first crack load, failure load, and deflection by 34.4%, 45.5%, and 56.04%, respectively. The mechanism of failure was separation at the level of the CJ. As soon as the first shear crack appeared, this beam failed quickly.

5- **Dowels Existence:**
Dense dowels significantly affected the initial crack load and deflection by -44.3% and -23.1%, respectively, while increasing the ultimate load by (5.8 %). The beam became less ductile as the interlocking mechanism between the concrete segments improved with adding the dowels, increasing the load resistance capacity of the beam. The dowels' usage insignificantly influenced the beam segments' ultimate load behavior; it insignificantly affected the first crack load (26.2%). Using dense dowels increased the beam's shearing capacity proportional to the number of dowels used.

4.2.Analytical Study

1- The analytical program's ultimate loads were lower than the experimental program's findings by 5.6 % -7.7 %.
2- The presence of the HCJ made the beam more ductile.
3- The crack patterns generated by the numerical analysis at the failure loading stage agreed well with the experimental failure results.
4- Stresses in steel secondary reinforcement for CB did not reach their yield point. The maximum stress reached was about 440 MPa, while the yield stress of the actual stirrups was 640 MPa, noticing that the stirrups exceeded their yield point in the experimental results.
5- According to the parametric study of experimental data, employing a high-strength concrete of 70 MPa resulted in a 47.0 % ultimate load above the experimental value with normal strength (28 MPa).
6- In a parametric study of experimental data, using 8 @100 mm with v =0.049 led to a 10.3 % ultimate load value, whereas using 2mm @125 mm with v = 0.0025 resulted in a 55.8 % reduction in ultimate load magnitude.

ACKNOWLEDGEMENTS

The authors are grateful for the financial support for this research by the Civil Engineering Department, College of Engineering, Al-Nahrain University. Postgraduate Research Grant (PGRG) No. 2/5/8838 on 11/7/2019).

REFERENCES

[1] Fintel M. **Handbook of Concrete Engineering.** New York: Van Nostrand Reinhold Company; 1985.

[2] Yousifani AH. **Investigation of the Behavior of Reinforced Concrete Beams with Construction Joints Using Nonlinear Three-Dimensional Finite Elements.** [M.Sc. Thesis]. Baghdad, Iraq: University of Technology; 2004.

[3] Alghazali HH, Myers JJ. **Shear Behavior of Full-Scale High Volume Fly Ash-Self Consolidating.** *Construction and Building Materials* 2017; **157**:161-171.

[4] Jabir HA, Salman TS, Mhalhal JM. **Effect of Construction Joints on the Behavior of Reinforced Concrete Beams.** *Journal of Engineering* 2017; **23**(5):47-60.

[5] Abbas AN, Al-Naely HK, Abdulzahra HH, Al-Khafaji ZS. **Structural Behavior of Reinforced Concrete Beams Having Construction Joints at Different Elevation.** *International Journal of Civil Engineering and Technology* 2018; **9**(13):712-720.

[6] Ismael MA, Hameed YM, Abd HJ. **Effect of Construction Joint on Structural Performance of Reinforced Self-Compacting Concrete Beams.** *International Journal of Civil Engineering and Technology* 2019; **10**(1):297-306.

[7] Ibrahim MS, Solomon Y, Demere A, Shiferaw A, Sultan A, Moges A, Dawit K. **Effect of Construction Joint on the Shear Behavior of Reinforced Concrete Beams.** *Fib Symposium*

Concrete Structures for Resilient Society 2020; China (Online).

[8] Mathew A, Nazeer M. **Flexural Behavior of Reinforced Concrete Beams with Construction Joints.** *International Research Journal of Engineering and Technology* 2020; **7**(6):3789-3796.

[9] Al-Rifaie A, Al-Hassani H, Shubbar AA. **Flexural Behavior of Reinforced Concrete Beams with Horizontal Construction Joints.** *IOP Conference Series: Materials Science and Engineering* 2021; **1090**:012003.

[10] Budi AS, Safitri E, Sangadji S, Kristiawan SA. **Shear Strength of HVFA-SCC Beams without Stirrups.** *Buildings* 2021; **11**(4):177.

[11] Iraqi Standard Specifications No. 5. **Portland Cement.** Baghdad, Iraq: Iraqi Central Organization for Standardization and Quality Control; 1984. (In Arabic)

[12] Iraqi Standard Specification No. 45. **Aggregate from Natural Sources for Concrete.** Baghdad, Iraq: The Iraqi Central Agency for Standardization and Quality Control; 1984. (In Arabic)

[13] EFNARC. **Specification and Guidelines for Self-Compacting Concrete.** Farnham, UK: EFNARC; 2002.

[14] ASTM C494/C494M-19. **Standard Specification for Chemical Admixtures for Concrete.** West Conshohocken, PA: ASTM International; 2019.

[15] ASTM A615/A615M-20. **Standard Specification for Deformed and Plain Carbon-Steel Bars for Concrete Reinforcement.** West Conshohocken, PA: ASTM International; 2020.

[16] Jasim AT. **Production of Self-Compacting Concrete Using Limestone.** *Journal of Kerbala University* 2011; **1**:87-100.

[17] Farhan OS. **Behavior of Self Compacting Concrete Deep Beams under Repeated Loading.** [Ph.D. Dissertation]. Baghdad, Iraq: Al-Nahrain University; 2014.

[18] ANSYS. **ANSYS Help.** Release 16.1.

[19] Gigar FZ. **Experimental Investigation of Construction Joints in RC Beams.** [M.Sc. Thesis]. Addis Ababa, Ethiopia: Addis Ababa University; 2015.

[20] Randl N. **Design Recommendations for Interface Shear Transfer in MC 2010.** *Structural Concrete* 2013; **14**(3): 230-241.

[21] Dawe DJ. **Matrix and Finite Element Displacement Analysis of Structures.** Oxford, UK: Clarendon Press; 1984.